energies

MDPI

Article

Optimized Takagi–Sugeno Fuzzy Mixed H_2/H_∞ Robust Controller Design Based on CPSOGSA Optimization Algorithm for Hydraulic Turbine Governing System

Lisheng Li [1], Jing Qian [1,*], Yidong Zou [1], Danning Tian [2], Yun Zeng [1], Fei Cao [1] and Xiang Li [1]

[1] School of Metallurgy and Energy Engineering, Kunming University of Science and Technology, Kunming 650093, China; lilisheng@stu.kust.edu.cn (L.L.); yidong@stu.kust.edu.cn (Y.Z.); zengyun001@163.com (Y.Z.); caofei@stu.kust.edu.cn (F.C.); lixiang9701@stu.kust.edu.cn (X.L.)
[2] School of Global Public Health, New York University, New York, NY 10012, USA; dt2354@nyu.edu
* Correspondence: qj0117@kust.edu.cn; Tel.: +86-137-0844-0678

Abstract: The hydraulic turbine governing system (HTGS) is a complex nonlinear system that regulates the rotational speed and power of a hydro-generator set. In this work, an incremental form of an HTGS nonlinear model was established and the Takagi–Sugeno (T-S) fuzzy linearization and mixed H_2/H_∞ robust control theory was applied to the design of an HTGS controller. A T-S fuzzy H_2/H_∞ controller for an HTGS based on modified hybrid particle swarm optimization and gravitational search algorithm integrated with chaotic maps (CPSOGSA) is proposed in this paper. The T-S fuzzy model of an HTGS that integrates multiple-state space equations was established by linearizing numerous equilibrium points. The linear matrix inequality (LMI) toolbox in MATLAB was used to solve the mixed H_2/H_∞ feedback coefficients using the CPSOGSA intelligent algorithm to optimize the weighting matrix in the process so that each mixed H_2/H_∞ feedback coefficients in the fuzzy control were optimized under the constraints to improve the performance of the controller. The simulation results show that this method allows the HTGS to perform well in suppressing system frequency deviations. In addition, the robustness of the method to system parameter variations is also verified.

Keywords: HTGS; T-S fuzzy; mixed H_2/H_∞ controller; CPSOGSA; wind power disturbances

Citation: Li, L.; Qian, J.; Zou, Y.; Tian, D.; Zeng, Y.; Cao, F.; Li, X. Optimized Takagi–Sugeno Fuzzy Mixed H_2/H_∞ Robust Controller Design Based on CPSOGSA Optimization Algorithm for Hydraulic Turbine Governing System. *Energies* **2022**, *15*, 4771. https://doi.org/10.3390/en15134771

Academic Editor: Helena M. Ramos

Received: 1 June 2022
Accepted: 27 June 2022
Published: 29 June 2022

1. Introduction

Clean, renewable energy generation, such as water, wind, and solar energy, is an effective means to cope with energy problems and environmental management issues. The proportion of clean, renewable energy in energy consumption will continue to increase. The development and full use of clean, efficient renewable energy and renewable energy generation are increasingly widely concerned by the international community [1,2]. At the same time, in some areas, there are hydroelectric power and wind power access to the same line because the wind speed is unstable; even if the wind turbine controller itself can reduce the impact of wind speed instability on the power, the wind power still has instability, causing some disturbance to the system frequency. Frequency is an important indicator of power quality and it is an essential requirement for power system operation to ensure that the system frequency is up to standard. Frequency is closely related to the rotational speed of the generator and in hydropower plants, the hydraulic turbine governing system (HTGS) is used to regulate the rotational speed of the unit. The HTGS is a complex control system integrating hydraulic, mechanical, and electrical components [3–5]. Its primary task is to regulate the active power output of the hydro-generator set according to the constant change of the load of the power system, minimize the influence of environmental disturbance and load disturbance, and maintain the frequency of the set within the specified range, which plays an indispensable role in maintaining the safe, stable, and economic operation of the

hydropower plant. However, the inertia of the flowing water in the penstock, the nonlinear characteristics of the hydro-generator set, and the load disturbance of the power system that occurs at any time make the control of the HTGS very difficult [6,7].

The problem of nonlinear modeling and control of the HTGS has been a topic of interest and has been studied in various aspects by related scholars. In the nonlinear modeling of the HTGS, a multi-machine differential equation model suitable for control design and stability analysis is established in [8]. Under different operating conditions of the HTGS, a non-linear mathematical model of the HTGS, considering the fractional derivative and time delay and during load rejection using non-linear dynamic transfer coefficients, is established respectively [9,10]. In the nonlinear control of the HTGS, proportional-integral-derivative (PID) control is the main controller of this system because of its simple structure and easy implementation. Some scholars have used different intelligent optimization algorithms to optimally adjust the parameters of the system controller under multiple objectives to improve the performance of the PID controller [11–13]. However, inevitably, the PID control method is not very adaptable to different working conditions nor resistant to disturbances. Therefore, many researchers have adopted some advanced intelligent control theories to optimize the control effect on the HTGS [14–17]. Nonlinear PID control, sliding mode control, model predictive control, Hamilton energy function method, and other nonlinear control applications have been applied to HTGS control problems, and all have achieved positive control results [18–21]. However, the above nonlinear modeling and control methods require a more in-depth mathematical foundation that is not easily mastered by most engineers and technicians.

In the field of control, Takagi–Sugeno (T-S) fuzzy control is a classical method that is easy to master [22]. It has been empirically and theoretically proven that T-S fuzzy models can approximate nonlinear systems with arbitrary accuracy by local state information and fuzzy rules [23]. In the literature [24], a robust analysis of a T-S fuzzy controller for the nonlinear system was carried out, showing that the robust fuzzy controller works well under the influence of model uncertainty, time lag, and large perturbations. The literature [25] shows the effectiveness of T-S fuzzy controllers based on the Lyapunov function and linear matrix inequality (LMI) for suppressing system disturbances. A systematic procedure of fuzzy control system design that consists of fuzzy model construction, rule reduction, and robust compensation for nonlinear systems was proposed in the literature [26], which can provide a reference for solving the fuzzy control design problem of nonlinear systems. Scholars can linearize the nonlinear HTGS mathematical model and combine it with appropriate fuzzy rules to construct a T-S fuzzy model based on which the controller is designed. A T-S fuzzy controller based on the fractional-order system robust theory [16] and finite-time stability theory was designed, respectively [27]. As we all know, the nonlinear term in the HTGS is mainly the power angle of the generator. However, the establishment of the T-S fuzzy model in [16,27,28] was based on the rotational speed as a prerequisite and the physical meaning of the fuzzy model established in this way is not clear. In the process of system response, the way that the T-S fuzzy system fits the original nonlinear system is not discussed in detail and in-depth in these papers.

With the large-scale grid connection of wind power and photovoltaic power generation, more and more factors affect the stable operation of the hydro-generator set. When the hydro-generator set is disturbed by random load, the state trajectory, in terms of power angle and rotational speed, exhibits instability, affecting the unit's stable operation. The system's stability is inseparable from the control parameters, which places high demands on the HTGS control parameters. Various parameter optimization algorithms currently have their advantages and disadvantages. Genetic algorithm (GA) has an excellent global search capability but poor local search capability and is prone to local minima [29]. Particle swarm optimization (PSO) has favorable searchability in the early iteration stage but poor searchability in the late stage [30]. Gravitational search algorithm (GSA) has a strong global search capability, but its local search capability is insufficient and it is prone to the

phenomenon of oscillation of optimal values. Therefore, there is an urgent need to study the parameter optimization techniques applicable to an HTGS controller.

From the above discussion, we were motivated to propose an optimal T-S fuzzy controller based on a suitable parameter optimization algorithm and study the control strategy for a nonlinear HTGS. The main contributions of this paper are reflected in the following: (1) the T-S fuzzy model of the HTGS was established with generator power angle as the precondition; (2) the mixed H_2/H_∞ controllers were integrated into T-S fuzzy control under the parallel distributed compensation (PDC); (3) these mixed H_2/H_∞ controllers were optimized using the modified hybrid particle swarm optimization and gravitational search algorithm integrated with chaotic maps (CPSOGSA) optimization algorithms to improve the performance of T-S fuzzy control; (4) the fuzzy control obtained by the optimization solution was applied to the HTGS.

The rest of this paper is organized as follows: Section 2 provides models of each component of the HTGS in incremental form, including the model of hydraulic turbine, penstock, actuator, and the nonlinear model of generator, which together form the nonlinear model of the HTGS. Section 3 demonstrates the T-S fuzzy local linearization of the nonlinear model of the HTGS through which three local linear models were obtained, and introduces three fuzzy control rules, which are linked together with fuzzy membership functions to form a T-S fuzzy controller. In Section 4, using the LMI toolbox in MATLAB, we propose our design of the mixed H_2/H_∞ controller for the fuzzy linear model introduced in Section 3. Section 5 presents a chaotic map-based PSOGSA optimization algorithm (CPSOGSA) as it was applied to parameter optimization of the mixed H_2/H_∞ controller. A simulation study was conducted and is shown in Section 6 to demonstrate the advantages of the new approach. Finally, concluding remarks are presented in Section 7.

2. System Description

An HTGS is a non-linear, multi-input, multi-output complex control system integrating hydraulic, mechanical, and electrical components, consisting of a hydraulic turbine, penstock, generator, and governor [10,31–33]. It has an important feature: its characteristics are related to the steady-state operating point. The structural diagram of the HTGS studied in this paper is shown in Figure 1. The upper part of Figure 1 is the general physical structure of the hydropower plant, which consists of upper and downstream reservoirs, hydrogenerator set, and penstock. The generator in it is driven by a hydroturbine. In order to maintain the power quality, it is necessary to keep the rotational speed of the generator stable. This part of the task is accomplished by adjusting the opening of the guide vanes by the actuator controlled by the governor. The lower part of Figure 1 is a block diagram of the HTGS that this paper focuses on, where the control quantity is the actual value, the power angle is the incremental value, and the remaining quantities are the relative values of the increments. To study the control strategy of the controller, each component of the HTGS needs to be modeled separately [20,23].

2.1. Hydraulic Turbine Model

For Francis turbines, five parameters are usually used to describe them: torque M_t, flow rate Q, water head H, rotational speed n, and guide vane opening $\boldsymbol{A}$. The torque and flow rate of the turbine are related to the water head, rotational speed, and guide vane opening [34]. Assuming an approximately linear relationship between the guide vane opening and the actuator stroke Y, the steady-state characteristics of the hydraulic turbine are now widely used to approximate the dynamic processes of the HTGS. M_r is the torque rating, Q_r is the flow rating, n_r is the rotational speed rating, H_r is the water head rating, and Y_{mAx} is the maximum value of the actuator stroke. For the steady-state operating point ($H(t) = H_0,\ n(t) = n_0,\ Y(t) = Y_0$), the nonlinear model of the hydraulic turbine in incremental form is obtained as shown in Equation (1) [35]:

$$\begin{cases} \Delta m_t(t) = \Delta m_t(\Delta x(t), \Delta y(t), \Delta h(t)) \\ \Delta q(t) = \Delta q(\Delta x(t), \Delta y(t), \Delta h(t)) \end{cases} \tag{1}$$

where $\Delta m_t(t) = [M_t(t) - M_t(n_0, Y_0, H_0)]/M_r$ is the relative value of torque increment, $\Delta q(t) = [Q(t) - Q(n_0, Y_0, H_0)]/Q_r$ is the relative value of flow increment, $\Delta x(t) = [n(t) - n_0]/n_r$ is the relative value of speed increment, $\Delta x(t) = n_*(t) - 1$ (subscript * indicates per unit value), $\Delta y(t) = [Y(t) - Y_0]/Y_{mAx}$ is the relative value of actuator stroke increment, and $\Delta h(t) = [H(t) - H_0]/H_r$ is the relative value of head increment.

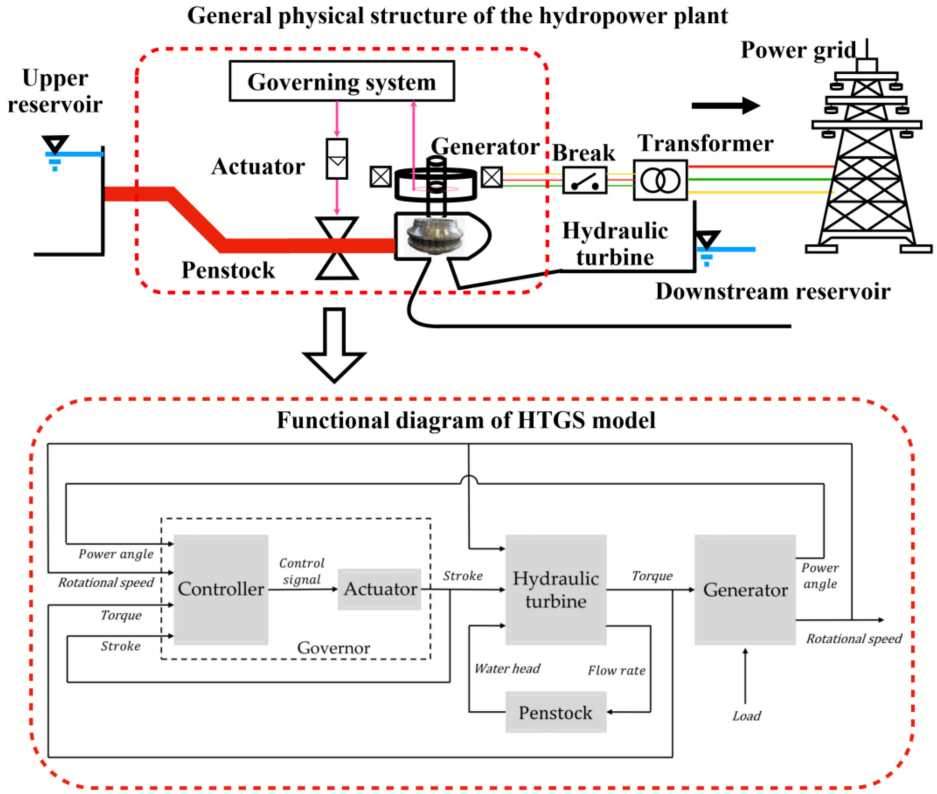

Figure 1. Structure of HTGS.

In studying the small disturbance problem, it can be linearized near the steady-state operating point. Expanding Equation (1) to Taylor series at the steady-state operating point and omitting the higher-order terms above the second order, a linearized model expressed in six transfer coefficients is obtained as Equation (2) [36]:

$$\begin{cases} \Delta m_t(t) = e_x \Delta x(t) + e_y \Delta y(t) + e_h \Delta h(t) \\ \Delta q(t) = e_{qx} \Delta x(t) + e_{qy} \Delta y(t) + e_{qh} \Delta h(t) \end{cases} \quad (2)$$

where, $e_x = \partial \Delta m_t(t)/\partial \Delta x(t)$, $e_y = \partial \Delta m_t(t)/\partial \Delta y(t)$, and $e_h = \partial \Delta m_t(t)/\partial \Delta h(t)$ are the transmission coefficients of turbine torque to rotational speed, stroke, and water head under steady-state conditions, respectively; $e_{qx} = \partial \Delta q(t)/\partial \Delta x(t)$, $e_{qy} = \partial \Delta q(t)/\partial \Delta y(t)$, and $e_{qh} = \partial \Delta q(t)/\partial \Delta h(t)$ are the transmission coefficients of turbine flow rate to rotational speed, stroke, and water head under steady-state conditions, respectively.

According to Equation (2), the linearized model of the hydraulic turbine is plotted in the form of the block diagram shown in Figure 2, where $G_h(s)$ is the transfer function of the penstock.

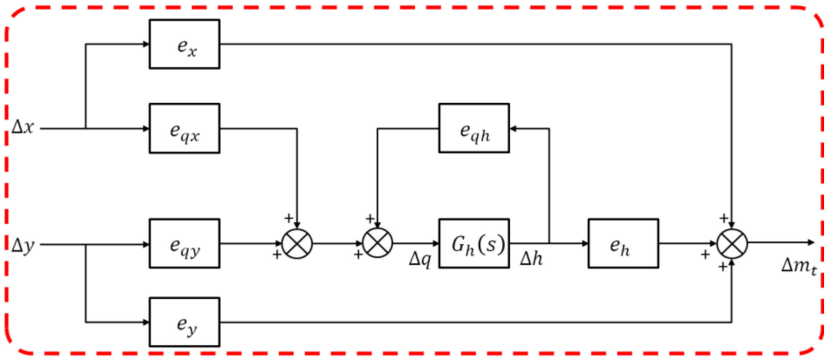

Figure 2. Linearized model of the hydraulic turbine.

2.2. Penstock Model

When the rotational speed changes in unstable conditions, the hydraulic turbine guide vane opening changes automatically under the action of the governor.

Water strike is a common phenomenon in this process, which is caused by the inertia of flowing water, compressibility, and the elasticity of the penstock. When the guide vane opening is increased, the increase in flow rate causes the working water pressure of the turbine to decrease. In the case of a large water hammer, the amount of torque decrease caused by the water pressure decrease exceeds the amount of torque increase caused by the flow increase, and the torque temporarily decreases. This counter-conditioning effect has a very negative impact on the dynamic characteristics of the HTGS. Thus, it is essential to analyze the dynamic characteristics of the penstock [37].

For the HTGS in minor fluctuation conditions, when the penstock length is less than 800 m, the compressibility of the flowing water and the elasticity of the penstock wall can be ignored. The penstock can be represented by the transfer function shown as Equation (3) [3]:

$$G_h(s) = \frac{\Delta h(s)}{\Delta q(s)} = -T_w \tag{3}$$

where T_w is the flowing water inertia time constant.

The corresponding differential equation model of the penstock is given as:

$$\frac{d\Delta q(t)}{dt} = -\frac{1}{T_w}\Delta h(t) \tag{4}$$

2.3. Generator Model

In this paper, the second-order model of the generator is shown as Equation (5), including the equation of rotor rotational motion and the equation characterizing the relation between power angle and rotational speed [16]:

$$\begin{cases} T_J \frac{d\omega_*(t)}{dt} = M_{t*}(t) - M_{e*}(t) - d(\omega_*(t) - 1) \\ \frac{d\delta(t)}{dt} = (\omega_*(t) - 1)\omega_0 \end{cases} \tag{5}$$

where T_J is the inertia time constant (s) of the unit, ω_* is the electrical angular velocity p.u.) of the generator, M_{t*} is the mechanical torque (p.u.) of the turbine, M_{e*} is the electromagnetic torque (p.u.) of the generator, d is the damping coefficient, δ is the power angle of the generator, and δ is taken to be 30° under steady-state conditions, i.e., $\delta_0 = 30°$, and δ changes when disturbance occurs; ω_0 is the synchronous electrical angular velocity.

The relationship between the generator's output power and the power angle is also considered. Assuming that the generator q-axis transient electromotive force E_q' remains constant during the disturbance and ignoring the stator winding losses, the electromagnetic

power P_{e*} (p.u.) supplied to the grid by the convex-pole synchronous generator is obtained as Equation (6) [38]:

$$P_{e*}(\mathrm{t}) = \frac{E'_{q*}V_{s*}}{X'_{d\Sigma*}}\sin\delta(t) + \frac{V_{s*}^2}{2}\cdot\frac{X'_{d\Sigma*} - X_{q\Sigma*}}{X'_{d\Sigma*}\,X_{q\Sigma*}}\sin 2\delta(t) \tag{6}$$

where V_{s*} is the bus voltage (p.u.); $X'_{d\Sigma*}$, $X_{q\Sigma*}$ are the sum of reactances (p.u.) in the d- axes and q-axes, respectively.

The generator model is now transformed into incremental form and the relationship between the correlated variables is as follows:

$$\omega_*(t) - 1 = n_*(t) - 1 = \Delta x(t) \tag{7}$$

$$\frac{d\omega_*(t)}{dt} = \frac{d[\Delta x(t) + 1]}{dt} = \frac{d\Delta x(t)}{dt} \tag{8}$$

$$\delta(t) = \delta_0 + \Delta\delta(t) \tag{9}$$

Because the electrical angular velocity is generally considered to vary little during the analysis of minor disturbances under grid-connected operation conditions, $\omega_*(t) = 1$ is taken so that:

$$P_{e*}(t) = M_{e*}(t) \tag{10}$$

Substituting Equations (7)–(10) into Equation (5) yields the second-order model of the generator in incremental form, as shown in Equation (11) [38]:

$$\begin{cases} \frac{d\Delta\delta(t)}{dt} = \omega_0\Delta x(t) \\ \frac{d\Delta x(t)}{dt} = \frac{1}{T_J}[\Delta m_t(t) - \Delta P_{e*}(t) - D\Delta x(t)] \end{cases} \tag{11}$$

where ΔP_{e*} is the per unit of the electromagnetic power increment, which is derived as follows:

$$\begin{aligned} &\Delta P_{e*}(t) = P_{e*}(t) - P_{e0*}(t) \\ &= \frac{E'_{q*}V_{s*}}{X'_{d\Sigma*}}\sin\delta_0\cdot\cos\Delta\delta(t) + \frac{E'_{q*}V_{s*}}{X'_{d\Sigma*}}\cos\delta_0\cdot\sin\Delta\delta(t) - V_{s*}^2\cdot\frac{X'_{d\Sigma*} - X_{q\Sigma*}}{X'_{d\Sigma*}\,X_{q\Sigma*}}\sin 2\delta_0\cdot\sin^2\Delta\delta(t) \\ &+V_{s*}^2\cdot\frac{X'_{d\Sigma*} - X_{q\Sigma*}}{X'_{d\Sigma*}\,X_{q\Sigma*}}\cos 2\delta_0\cdot\sin\Delta\delta(t)\Delta\cdot\cos\Delta\delta(t) - \frac{E'_{q*}V_{s*}}{X'_{d\Sigma*}}\sin\delta_0 \end{aligned} \tag{12}$$

2.4. Actuator Model

The actuator of the HTGS generally adopts the electro-hydraulic follower system, whose function is to amplify the control signal and provide the execution power to convert the weak electrical control signal from the controller into a mechanical displacement signal that can drive the hydraulic turbine guide vane. When the nonlinear factors are ignored, the actuator can be simplified to a first-order inertial element [14], whose transfer function [39] can be expressed as:

$$G_y(s) = \frac{\Delta y(s)}{u(s)} = \frac{1}{T_y s + 1} \tag{13}$$

where T_y is the actuator response time constant.

The corresponding differential equation model of the actuator [36] is given as:

$$\frac{d\Delta y(t)}{dt} = -\frac{1}{T_y}\Delta y(t) + \frac{1}{T_y}u(t) \tag{14}$$

To avoid the system scattering phenomenon caused by the actuator saturation, we designed the actuator with anti-integration saturation in the simulation. The integration

stops when the actuator's output reaches saturation and the sign of the control quantity is the same as the sign of the actuator's output.

2.5. HTGS Model

The transfer function from Δy to Δm_t which derived from Figure 2, is shown as Equation (15):

$$G_{ym}(s) = \frac{\Delta m_t(s)}{\Delta y(s)} = \frac{e_y + \left(e_{qy}e_h - e_{qh}e_y\right)G_h(s)}{1 - e_{qh}G_h(s)} \tag{15}$$

Let:

$$e = \frac{e_{qy}e_h}{e_y} - e_{qh} \tag{16}$$

Then:

$$G_{ym}(s) = \frac{\Delta m_t(s)}{\Delta y(s)} = e_y\frac{1 + eG_h(s)}{1 - e_{qh}G_h(s)} \tag{17}$$

Substituting Equation (3) into Equation (17) yields:

$$\Delta m_t(s)\left(1 + e_{qh}T_w s\right) = \Delta y(s)\left(e_y - e_y e T_w s\right) \tag{18}$$

The inverse Laplace transform of Equation (18) yields:

$$\frac{d\Delta m_t(t)}{dt} = \frac{1}{e_{qh}T_w}\left(e_y\Delta y(t) - \Delta m_t(t) - e_y e T_w\frac{d\Delta y(t)}{dt}\right) \tag{19}$$

Substituting Equation (14) into Equation (19) yields:

$$\frac{d\Delta m_t(t)}{dt} = \frac{1}{e_{qh}T_w}\left[-\Delta m_t(t) + \left(e_y + e_y e\frac{T_w}{T_y}\right)\Delta y(t) - e_y e\frac{T_w}{T_y}u(t)\right] \tag{20}$$

Equations (11), (14) and (20) constitute the model of the HTGS, which is shown as Equation (21):

$$\begin{cases} \frac{d\Delta\delta(t)}{dt} = \omega_0\Delta x(t) \\ \frac{d\Delta x(t)}{dt} = \frac{1}{T_J}[\Delta m_t(t) - \Delta P_{e*}(t) - D\Delta x(t)] \\ \frac{d\Delta m_t(t)}{dt} = \frac{1}{e_{qh}T_w}\left[-\Delta m_t(t) + \left(e_y + e_y e\frac{T_w}{T_y}\right)\Delta y(t) - e_y e\frac{T_w}{T_y}u(t)\right] \\ \frac{d\Delta y(t)}{dt} = -\frac{1}{T_y}\Delta y(t) + \frac{1}{T_y}u(t) \end{cases} \tag{21}$$

where ΔP_{e*} is a nonlinear term on the variable $\Delta\delta$, whose expression is shown in Equation (12).

3. T-S Fuzzy Local Linearization and Controller Proposal

The T-S fuzzy model has a wide range of applications in control design and analysis of nonlinear systems [40], which is easy to understand, convenient, and flexible for engineering applications. Its main feature is described by some If-Then fuzzy inference rules; each inference rule represents the dynamics of the local area linear model and then the individual local linear models are linked with fuzzy membership functions to obtain the overall fuzzy nonlinear model, which in turn achieves the purpose of control design for nonlinear uncertain systems [28]. In this section, the T-S fuzzy local linearization of the nonlinear model of the HTGS is carried out to obtain three local linear models and the three fuzzy control rules are proposed. They are linked together with fuzzy membership functions to form a T-S fuzzy controller.

$\Delta\delta(t)$, $\Delta x(t)$, $\Delta m_t(t)$, and $\Delta y(t)$ are selected as state variables and Equation (21) is transformed into the matrix form of the HTGS model as follows:

$$\frac{d\boldsymbol{x}(t)}{dt} = \boldsymbol{\mathcal{F}}(\boldsymbol{x}(t)) + \boldsymbol{B}_u u(t) \tag{22}$$

where

$$\boldsymbol{x}(t) = \begin{bmatrix} x_1(t) & x_2(t) & x_3(t) & x_4(t) \end{bmatrix}^T = \begin{bmatrix} \Delta\delta(t) & \Delta x(t) & \Delta m_t(t) & \Delta y(t) \end{bmatrix}^T \tag{23}$$

$$\boldsymbol{\mathcal{F}}(\boldsymbol{x}(t)) = \begin{bmatrix} \omega_0 x_2(t) \\ -\frac{1}{T_J} \cdot \Delta P(x_1(t)) - \frac{D}{T_J} x_2(t) + \frac{1}{T_J} x_3(t) \\ -\frac{1}{e_{qh} T_w} x_3(t) + \frac{e_y}{e_{qh} T_w} \left(1 + e \frac{T_w}{T_y}\right) x_4(t) \\ -\frac{1}{T_y} x_4(t) \end{bmatrix} \tag{24}$$

$$\begin{aligned} \Delta\mathcal{P}(x_1(t)) \quad &= \frac{E_q' V_s}{X_{d\Sigma}'} \sin\delta_0 \cdot \cos x_1(t) + \frac{E_q' V_s}{X_{d\Sigma}'} \cos\delta_0 \cdot \sin x_1(t) - V_s^2 \cdot \frac{X_{d\Sigma}' - X_{q\Sigma}}{X_{d\Sigma}' X_{q\Sigma}} \sin 2\delta_0 \cdot \sin^2 x_1(t) - \frac{E_q' V_s}{X_{d\Sigma}'} \sin\delta_0 \\ &+ V_s^2 \cdot \frac{X_{d\Sigma}' - X_{q\Sigma}}{X_{d\Sigma}' X_{q\Sigma}} \cos 2\delta_0 \cdot \sin x_1(t) \cdot \cos x_1(t) \end{aligned} \tag{25}$$

$$\boldsymbol{B}_u = \begin{bmatrix} 0 & 0 & -\frac{e_y e}{e_{qh} T_y} & \frac{1}{T_y} \end{bmatrix}^T \tag{26}$$

where $\boldsymbol{B}_u$ is the coefficient matrix of the control input.

$\delta_0 = 30^\circ$. Considering the boundedness of x_1 ($x_1 \in [-\mathrm{d}, \mathrm{d}]$, taking $\mathrm{d} = \pi/6$), the T-S fuzzy model of the system is established. When $x_1(t) \to 0$, then $\sin x_1(t) \to x_1(t)$, $\sin^2 x_1(t) \to 0$, $x_1(t) \to 1$; when $x_1(t) \to \pi/6$, then $\sin x_1(t) \to \sin(\pi/6) = 0.5 \to (3/\pi)x_1(t)$, $\cos x_1(t) \to \cos(\pi/6) = \sqrt{3}/2 \to \left(3\sqrt{3}/\pi\right)x_1(t)$; when $x_1(t) \to -\pi/6$, then $\sin x_1(t) \to -\sin(\pi/6) = -0.5 \to (3/\pi)x_1(t)$, and $\cos x_1(t) \to \cos(\pi/6) = \sqrt{3}/2 \to \left(-3\sqrt{3}/\pi\right)x_1(t)$. This leads to the following three T-S fuzzy rules.

3.1. Fuzzy Local Linearization

Fuzzy rule 1: If $x_1(t)$ is about 0, then fuzzy model 1 is shown as Equation (27):

$$\frac{d\boldsymbol{x}(t)}{dt} = \boldsymbol{A}^{(1)}\boldsymbol{x}(t) + \boldsymbol{B}_u^{(1)} u(t) \tag{27}$$

where

$$\boldsymbol{A}^{(1)} = \begin{bmatrix} 0 & \omega_0 & 0 & 0 \\ S_1 & -\frac{D}{T_J} & \frac{1}{T_J} & 0 \\ 0 & 0 & -\frac{1}{e_{qh} T_w} & \frac{e_y}{e_{qh} T_w}\left(1 + e\frac{T_w}{T_y}\right) \\ 0 & 0 & 0 & -\frac{1}{T_y} \end{bmatrix} \tag{28}$$

$$\boldsymbol{B}_u^{(1)} = \boldsymbol{B}_u = \begin{bmatrix} 0 & 0 & -\frac{e_y e}{e_{qh} T_y} & \frac{1}{T_y} \end{bmatrix}^T \tag{29}$$

at this point,

$$\Delta\mathcal{P}(x_1(t)) = \left(\frac{E_q' V_s}{X_{d\Sigma}'} \cos\delta_0 + V_s^2 \cdot \frac{X_{d\Sigma}' - X_{q\Sigma}}{X_{d\Sigma}' X_{q\Sigma}} \cos 2\delta_0\right) x_1(t) \tag{30}$$

$$S_1 = -\frac{1}{T_J}\left(\frac{E_q' V_s}{X_{d\Sigma}'} \cos\delta_0 + V_s^2 \cdot \frac{X_{d\Sigma}' - X_{q\Sigma}}{X_{d\Sigma}' X_{q\Sigma}} \cos 2\delta_0\right) \tag{31}$$

Fuzzy rule 2: If $x_1(t)$ is about $\pi/6$, then fuzzy model 2 is shown as Equation (32):

$$\frac{d\boldsymbol{x}(t)}{dt} = \boldsymbol{A}^{(2)}\boldsymbol{x}(t) + \boldsymbol{B}_u^{(2)}u(t) \tag{32}$$

where

$$\boldsymbol{A}^{(2)} = \begin{bmatrix} 0 & \omega_0 & 0 & 0 \\ S_2 & -\frac{D}{T_J} & \frac{1}{T_J} & 0 \\ 0 & 0 & -\frac{1}{e_{qh}T_w} & \frac{e_y}{e_{qh}T_w}\left(1 + e\frac{T_w}{T_y}\right) \\ 0 & 0 & 0 & -\frac{1}{T_y} \end{bmatrix} \tag{33}$$

$$\boldsymbol{B}_u^{(2)} = \boldsymbol{B}_u = \begin{bmatrix} 0 & 0 & -\frac{e_y e}{e_{qh}T_y} & \frac{1}{T_y} \end{bmatrix}^T \tag{34}$$

at this point,

$$\Delta\mathcal{P}(x_1(t)) = \left(\frac{3\sqrt{3}-6}{\pi}\cdot\frac{E_q^{'}V_s}{X_{d\Sigma}^{'}}\sin\delta_0 + \frac{3}{\pi}\cdot\frac{E_q^{'}V_s}{X_{d\Sigma}^{'}}\cos\delta_0 - \frac{3V_s^2}{2\pi}\cdot\frac{X_{d\Sigma}^{'}-X_{q\Sigma}}{X_{d\Sigma}^{'}X_{q\Sigma}}\sin 2\delta_0 + \frac{3\sqrt{3}V_s^2}{2\pi}\cdot\frac{X_{d\Sigma}^{'}-X_{q\Sigma}}{X_{d\Sigma}^{'}X_{q\Sigma}}\cos 2\delta_0\right)x_1(t) \tag{35}$$

$$S_2 = -\frac{1}{T_J}\left(\frac{3\sqrt{3}-6}{\pi}\cdot\frac{E_q^{'}V_s}{X_{d\Sigma}^{'}}\sin\delta_0 + \frac{3}{\pi}\cdot\frac{E_q^{'}V_s}{X_{d\Sigma}^{'}}\cos\delta_0 - \frac{3V_s^2}{2\pi}\cdot\frac{X_{d\Sigma}^{'}-X_{q\Sigma}}{X_{d\Sigma}^{'}X_{q\Sigma}}\sin 2\delta_0 + \frac{3\sqrt{3}V_s^2}{2\pi}\cdot\frac{X_{d\Sigma}^{'}-X_{q\Sigma}}{X_{d\Sigma}^{'}X_{q\Sigma}}\cos 2\delta_0\right) \tag{36}$$

Fuzzy rule 3: If $x_1(t)$ is about $-\pi/6$, then fuzzy model 3 is shown as Equation (37):

$$\frac{dx(t)}{dt} = \boldsymbol{A}^{(3)}x(t) + \boldsymbol{B}_u^{(3)}u(t) \tag{37}$$

where

$$\boldsymbol{A}^{(3)} = \begin{bmatrix} 0 & \omega_0 & 0 & 0 \\ S_3 & -\frac{D}{T_J} & \frac{1}{T_J} & 0 \\ 0 & 0 & -\frac{1}{e_{qh}T_w} & \frac{e_y}{e_{qh}T_w}\left(1 + e\frac{T_w}{T_y}\right) \\ 0 & 0 & 0 & -\frac{1}{T_y} \end{bmatrix} \tag{38}$$

$$\boldsymbol{B}_u^{(3)} = \boldsymbol{B}_u = \begin{bmatrix} 0 & 0 & -\frac{e_y e}{e_{qh}T_y} & \frac{1}{T_y} \end{bmatrix}^T \tag{39}$$

at this point,

$$\Delta\mathcal{P}(x_1(t)) = \left(\frac{6-3\sqrt{3}}{\pi}\cdot\frac{E_q^{'}V_s}{X_{d\Sigma}^{'}}\sin\delta_0 + \frac{3}{\pi}\cdot\frac{E_q^{'}V_s}{X_{d\Sigma}^{'}}\cos\delta_0 + \frac{3V_s^2}{2\pi}\cdot\frac{X_{d\Sigma}^{'}-X_{q\Sigma}}{X_{d\Sigma}^{'}X_{q\Sigma}}\sin 2\delta_0 + \frac{3\sqrt{3}V_s^2}{2\pi}\cdot\frac{X_{d\Sigma}^{'}-X_{q\Sigma}}{X_{d\Sigma}^{'}X_{q\Sigma}}\cos 2\delta_0\right)x_1(t) \tag{40}$$

$$S_3 = -\frac{1}{T_J}\left(\frac{6-3\sqrt{3}}{\pi}\cdot\frac{E_q^{'}V_s}{X_{d\Sigma}^{'}}\sin\delta_0 + \frac{3}{\pi}\cdot\frac{E_q^{'}V_s}{X_{d\Sigma}^{'}}\cos\delta_0 + \frac{3V_s^2}{2\pi}\cdot\frac{X_{d\Sigma}^{'}-X_{q\Sigma}}{X_{d\Sigma}^{'}X_{q\Sigma}}\sin 2\delta_0 + \frac{3\sqrt{3}V_s^2}{2\pi}\cdot\frac{X_{d\Sigma}^{'}-X_{q\Sigma}}{X_{d\Sigma}^{'}X_{q\Sigma}}\cos 2\delta_0\right) \tag{41}$$

3.2. T-S Fuzzy Controller

Design the following three fuzzy control rules:

$$\begin{cases} \text{Fuzzy control rules 1 : if } x_1(t) \text{ is about 0, then } u(t) = \boldsymbol{K}_1\boldsymbol{x}(t) \\ \text{Fuzzy control rules 2 : if } x_1(t) \text{ is about } \pi/6, \text{ then } u(t) = \boldsymbol{K}_2\boldsymbol{x}(t) \\ \text{Fuzzy control rules 3 : } if\ x_1(t) \text{ is about } -\pi/6, \text{ then } u(t) = \boldsymbol{K}_3\boldsymbol{x}(t) \end{cases} \tag{42}$$

where $\boldsymbol{K}_1$, $\boldsymbol{K}_2$, and $\boldsymbol{K}_3$ are the feedback gain matrices of the three locally stabilized controllers:

$$\begin{cases} \boldsymbol{K}_1 = \begin{bmatrix} K_{11} & K_{12} & K_{13} & K_{14} \end{bmatrix} \\ \boldsymbol{K}_2 = \begin{bmatrix} K_{21} & K_{22} & K_{23} & K_{24} \end{bmatrix} \\ \boldsymbol{K}_3 = \begin{bmatrix} K_{31} & K_{32} & K_{33} & K_{34} \end{bmatrix} \end{cases} \tag{43}$$

The T-S fuzzy state feedback controller of the design governor according to the parallel distribution compensation (PDC) algorithm is shown as Equation (44):

$$u(t) = w_1(x_1(t))\boldsymbol{K}_1\boldsymbol{x}(t) + w_2(x_1(t))\boldsymbol{K}_2\boldsymbol{x}(t) + w_3(x_1(t))\boldsymbol{K}_3\boldsymbol{x}(t) \tag{44}$$

where w_1, w_2, and w_3 are the membership degrees of x_1 to the first, second, and third fuzzy rules, respectively, and $w_1 + w_2 + w_3 = 1$. The degree of membership functions are shown as follows:

$$w_1(x_1(t)) = 1 - \frac{|x_1(t)|}{\pi/6} \; x_1(t) \in (-\pi/6, \; \pi/6) \tag{45}$$

$$w_2(x_1(t)) = \begin{cases} 0 \; x_1(t) \in (-\pi/6, 0) \\ \frac{x_1(t)}{\pi/6} \; x_1(t) \in (0, \pi/6) \end{cases} \tag{46}$$

$$\mathrm{w_3(x_1(t))} = \begin{cases} -\frac{x_1(t)}{\pi/6} \; x_1(t) \in (-\pi/6, 0) \\ 0 \; x_1(t) \in (0, \pi/6) \end{cases} \tag{47}$$

The degree of membership functions are shown schematically in Figure 3:

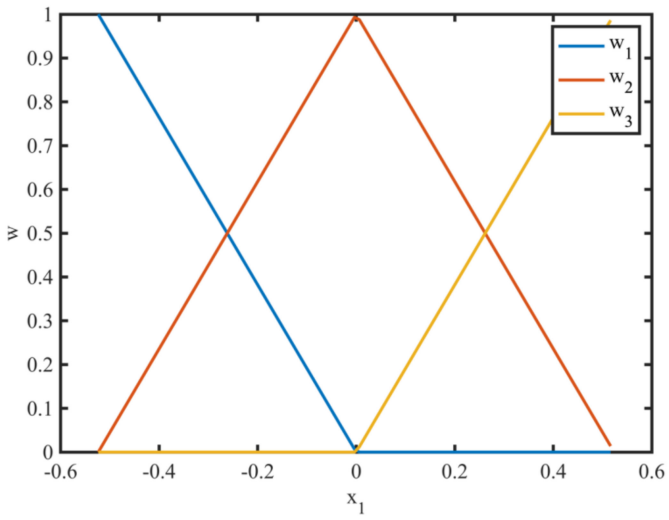

Figure 3. Diagram showing degree of membership function.

4. Design of the Mixed H_2/H_∞ Controller

For the fuzzy linear model i $(i = 1 \sim 3)$ in Section 3, designing a state feedback controller $u(t) = \boldsymbol{K}_i\boldsymbol{x}(t)$ is the problem to be solved in this section.

Equation (48) is the linear model corresponding to the fuzzy rule i:

$$\begin{cases} \frac{d\boldsymbol{x}(t)}{dt} = \boldsymbol{A}^{(i)}x(t) + \boldsymbol{B}_\omega^{(i)}\omega(t) + \boldsymbol{B}_u^{(i)}u(t) \\ \mathbf{z}_\infty^{(i)} = \boldsymbol{C}_1^{(i)}x(t) + \boldsymbol{D}_{11}^{(i)}\omega(t) + \boldsymbol{D}_{12}^{(i)}u(t) \;\; (i = 1 \sim 3) \\ \mathbf{z}_2^{(i)} = \boldsymbol{C}_2^{(i)}x(t) + \boldsymbol{D}_{21}^{(i)}\omega(t) + \boldsymbol{D}_{22}^{(i)}u(t) \end{cases} \tag{48}$$

where $\omega(t)$ is the disturbance signal, including the disturbance caused by the disturbance torque and the modeling error; take $\boldsymbol{B}_\omega^{(i)} = \begin{bmatrix} 0 & 0.1 & 0 & 0 \end{bmatrix}^{\mathrm{T}}$ as the disturbance signal coefficient matrix; $\mathbf{z}_\infty^{(i)}$ and $\mathbf{z}_2^{(i)}$ are the defined dynamic performance evaluation signals; and

$\boldsymbol{C}_1^{(i)}$, $\boldsymbol{C}_2^{(i)}$, $\boldsymbol{D}_{11}^{(i)}$, $\boldsymbol{D}_{12}^{(i)}$, $\boldsymbol{D}_{21}^{(i)}$, and $\boldsymbol{D}_{22}^{(i)}$ are the dimensionally appropriate weighting matrices. Optimizing the weighting matrix is the difficult part of the mixed H_2/H_∞ control. There is no well-established theory on how to select the weighting matrix. Generally, the main diagonal element has more influence on the controller and several attempts are needed to choose the optimal weighting matrix.

Define the correlation coefficient matrix in this paper as follows:

$$\boldsymbol{C}_1^{(i)} = \begin{bmatrix} \mu_1^{(i)} & 0 & 0 & 0 \\ 0 & \mu_2^{(i)} & 0 & 0 \\ 0 & 0 & \mu_3^{(i)} & 0 \\ 0 & 0 & 0 & \mu_4^{(i)} \end{bmatrix} \tag{49}$$

$$\boldsymbol{D}_{11}^{(i)} = \begin{bmatrix} 0 & 0 & 0 & 0 \end{bmatrix}^T \tag{50}$$

$$\boldsymbol{D}_{12}^{(i)} = \begin{bmatrix} 0 & 0 & 0 & \mu_5^{(i)} \end{bmatrix}^T \tag{51}$$

$$\boldsymbol{C}_2^{(i)} = \begin{bmatrix} \mu_6^{(i)} & 0 & 0 & 0 \\ 0 & \mu_7^{(i)} & 0 & 0 \\ 0 & 0 & \mu_8^{(i)} & 0 \\ 0 & 0 & 0 & \mu_9^{(i)} \end{bmatrix} \tag{52}$$

$$\boldsymbol{D}_{21}^{(i)} = \begin{bmatrix} 0 & 0 & 0 & 0 \end{bmatrix}^T \tag{53}$$

$$\boldsymbol{D}_{22}^{(i)} = \begin{bmatrix} 0 & 0 & 0 & \mu_{10}^{(i)} \end{bmatrix}^T \tag{54}$$

where $\mu_1^{(i)} \sim \mu_{10}^{(i)}$ are the weighting coefficients and the intelligent optimization algorithm will be used in Section 5 to find the optimal weighting coefficients several times and select the combination of weighting coefficients with optimal performance.

The system in Equation (48) can be represented as the control system in Figure 4. We aimed to design a controller with a feedback coefficient $\boldsymbol{K}_i$ such that the closed-loop system is asymptotically stable and the H_∞ norm of the closed-loop transfer function $T_{i\infty}(s)$ from ω to $\mathbf{z}_\infty^{(i)}$ does not exceed a given upper bound γ_{i0}, ensuring that the closed-loop system is robust to the uncertainty perturbations entering the system from ω, and such that the H_2 norm of the closed-loop transfer function $T_{i2}(s)$ from ω to $\mathbf{z}_2^{(i)}$ does not exceed a given upper bound ν_{i0}, ensuring that the system performance measured with the H_2 norm is at a good level [41].

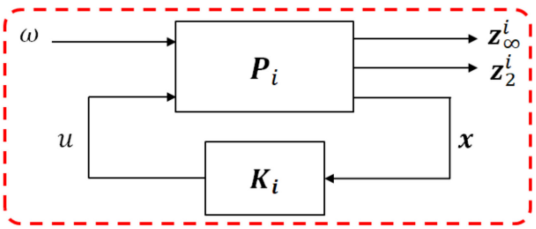

Figure 4. State feedback control.

From Equation (48), the augmented controlled object based on the mixed H_2/H_∞ control theory can be obtained as Equation (55):

$$P_i = \begin{bmatrix} \boldsymbol{A}^{(i)} & \boldsymbol{B}_\omega^{(i)} & \boldsymbol{B}_u^{(i)} \\ \boldsymbol{C}_1^{(i)} & \boldsymbol{D}_{11}^{(i)} & \boldsymbol{D}_{12}^{(i)} \\ \boldsymbol{C}_2^{(i)} & \boldsymbol{D}_{21}^{(i)} & \boldsymbol{D}_{22}^{(i)} \end{bmatrix} \tag{55}$$

The linear matrix inequality (LMI) toolbox in MATLAB provides a solution for the mixed H_2/H_∞ control problem, which can solve the feedback coefficient $\boldsymbol{K}_i$ of the mixed H_2/H_∞ state feedback controller $u(t) = \boldsymbol{K}_i\boldsymbol{x}(t)$ shown in Figure 3. The closed-loop system can be made stable for all parameter perturbation and external disturbances and the following performance specifications can be achieved.

1. H_∞-optimal design;

$$\|T_{i\infty}\|_\infty = \sup_\omega \sigma[T_{i\infty}(\mathrm{j}\omega)] < \gamma_{i0} \tag{56}$$

That is the H_∞ norm minimization, which is the peak minimization of the maximum singular value of the system frequency response. Then, the LMI is used to complete the design objective set in Equation (56), i.e., if and only if there exists a symmetric matrix $\boldsymbol{X}_{i\infty} > 0$, such that:

$$\begin{bmatrix} \left(\boldsymbol{A}^{(i)} + \boldsymbol{B}_u^{(i)}\boldsymbol{K}_i\right)\boldsymbol{X}_{i\infty} + \boldsymbol{X}_{i\infty}\left(\boldsymbol{A}^{(i)} + \boldsymbol{B}_u^{(i)}\boldsymbol{K}_i\right)^T & \boldsymbol{B}_\omega^{(i)} & \boldsymbol{X}_{i\infty}\left(\boldsymbol{C}_1^{(i)} + \boldsymbol{D}_{12}^{(i)}\boldsymbol{K}_i\right)^T \\ \boldsymbol{B}_\omega^{(i)T} & -\boldsymbol{I} & \boldsymbol{D}_{11}^{(i)T} \\ \left(\boldsymbol{C}_1^{(i)} + \boldsymbol{D}_{12}^{(i)}\boldsymbol{K}_i\right)\boldsymbol{X}_{i\infty} & \boldsymbol{D}_{11}^{(i)} & -\gamma_i^2\boldsymbol{I} \end{bmatrix} < 0 \tag{57}$$

2. H_2-optimal design;

$$\|T_{i2}\|_2 = \left(\frac{1}{2\pi}\int_{-\infty}^{\infty} \mathrm{trace}\left[T_{i2}^T(\mathrm{j}\omega)\right]d\omega\right)^{\frac{1}{2}} < \nu_{i0} \tag{58}$$

That is the H_2 norm minimization. Similarly, to accomplish the design goal shown in Equation (58), the inequality shown in Equation (59) is satisfied if and only if there exist symmetric matrices $\boldsymbol{X}_{i2}$ and $\boldsymbol{Q}_i$.

$$\begin{cases} \begin{bmatrix} \left(\boldsymbol{A}^{(i)} + \boldsymbol{B}_u^{(i)}\boldsymbol{K}_i\right)\boldsymbol{X}_{i2} + \boldsymbol{X}_{i2}\left(\boldsymbol{A}^{(i)} + \boldsymbol{B}_u^{(i)}\boldsymbol{K}_i\right)^T & \boldsymbol{B}_\omega^{(i)} \\ \boldsymbol{B}_\omega^{(i)T} & -\mathrm{I} \end{bmatrix} < 0 \\ \begin{bmatrix} \boldsymbol{Q}_i & \left(\boldsymbol{C}_2^{(i)} + \boldsymbol{D}_{22}^{(i)}\boldsymbol{K}_i\right)\boldsymbol{X}_{i2} \\ \boldsymbol{X}_{i2}\left(\boldsymbol{C}_2^{(i)} + \boldsymbol{D}_{22}^{(i)}\boldsymbol{K}_i\right)^T & \boldsymbol{X}_{i2} \end{bmatrix} > 0 \\ \mathrm{trace}(\boldsymbol{Q}_i) < v_i^2 \end{cases} \tag{59}$$

3. Mixed H_2/H_∞-optimal design.

Every state feedback controller in the T-S fuzzy system of the HTGS makes the closed-loop poles of the system lie in the left half-open complex plane and minimizes $\alpha\|T_{i\infty}\|_\infty^2 + \beta\|T_{i2}\|_2^2$ [42]. Then, the above two sets of conditions add up to the nonconvex optimization problem with variables $\boldsymbol{Q}_i$, $\boldsymbol{K}_i$, $\boldsymbol{X}_{i\infty}$, and $\boldsymbol{X}_{i2}$. For tractability in the LMI framework, we sought a single matrix $\boldsymbol{X}_i = \boldsymbol{X}_{i\infty} = \boldsymbol{X}_{i2}$ that enforces all two objectives. The change of variable $\boldsymbol{Y}_i = \boldsymbol{K}_i\boldsymbol{X}_i$ allows the following suboptimal LMI problem for multi-objective state feedback control to be solved.

Minimize $\alpha\|T_{i\infty}\|_\infty^2 + \beta\|T_{i2}\|_2^2$ by $\boldsymbol{Y}_i$, $\boldsymbol{X}_i$, $\boldsymbol{Q}_i$, and γ_i^2 satisfying Equation (60):

$$\begin{cases} \begin{bmatrix} \boldsymbol{A}^{(i)}\boldsymbol{X}_i + \boldsymbol{X}_i\boldsymbol{A}^{(i)T} + \boldsymbol{B}_u^{(i)}\boldsymbol{Y}_i + \boldsymbol{Y}_i^T\boldsymbol{B}_u^{(i)T} & \boldsymbol{B}_\omega^{(i)} & \boldsymbol{X}_i\boldsymbol{C}_1^{(i)T} + \boldsymbol{Y}_i^T\boldsymbol{D}_{12}^{(i)T} \\ \boldsymbol{B}_\omega^{(i)T} & -\boldsymbol{I} & \boldsymbol{D}_{11}^{(i)T} \\ \boldsymbol{C}_1^{(i)}\boldsymbol{X}_i + \boldsymbol{D}_{12}^{(i)}\boldsymbol{Y}_i & \boldsymbol{D}_{11}^{(i)} & -\gamma_i^2\boldsymbol{I} \end{bmatrix} < 0 \\ \begin{bmatrix} \boldsymbol{Q}_i & \boldsymbol{C}_2^{(i)}\boldsymbol{X}_i + \boldsymbol{D}_{22}^{(i)}\boldsymbol{Y}_i \\ \boldsymbol{X}_i\boldsymbol{C}_2^{(i)T} + \boldsymbol{Y}_i^T\boldsymbol{D}_{22}^{(i)T} & \boldsymbol{X}_i \end{bmatrix} > 0 \\ \mathrm{trace}(\boldsymbol{Q}_i) < v_{i0}^2 \\ \gamma_i^2 < \gamma_{i0}^2 \end{cases} \tag{60}$$

From the optimal solution $\boldsymbol{Y}_i^*$, $\boldsymbol{X}_i^*$, $\boldsymbol{Q}_i^*$, γ_i^*, the corresponding every state feedback gain $\boldsymbol{K}_i^*$ is given by Equation (61):

$$\boldsymbol{K}_i^* = \boldsymbol{Y}_i^*(\boldsymbol{X}_i^*)^{-1} \tag{61}$$

5. A Chaotic Map-Based Improved PSOGSA Optimization Algorithm (CPSOGSA) and Its Application in HTGS

Particle swarm optimization (PSO) and gravitational search algorithm (GSA) are discussed in this section, and the CPSOGSA algorithm, which improves on the previous two, is discussed. Finally, the procedure for finding the optimal feedback coefficient $\boldsymbol{K}_i$ for the state feedback controller $u(t) = \boldsymbol{K}_i\boldsymbol{x}(t)$ is given.

5.1. Particle Swarm Optimization

Particle swarm optimization (PSO) is an optimization algorithm for population intelligence in computational intelligence, which Kennedy and Eberhart proposed. The PSO algorithm originated from the study of the predatory behavior of birds [43]. The PSO algorithm first initializes a group of particles in the feasible solution space, representing a potential optimal solution to the extreme value optimization problem. It represents the particle characteristics by three indicators: position, velocity, and fitness value, and the fitness value is calculated by the fitness function [44], whose value is good or bad to indicate the superiority or inferiority of the particle. The particle moves in the solution space and updates the personal position by tracking the personal extremum pbest and the group extremum gbest. The fitness value is calculated once for each updated particle position. The personal extremum value pbest and group extremum value gbest positions are updated by comparing the fitness value of the new particle with the fitness values of the personal extremum value and group extremum value.

The velocity and position of each particle in the PSO algorithm are updated as follows:

$$\begin{cases} v_i(k+1) = wv_i(k) + c_1\cdot\mathrm{rand}\cdot(\ \mathrm{pbest}\ _i - p_i(k)) + c_2\cdot\mathrm{rand}\cdot(\ \mathrm{gbest}\ _i - p_i(k)) \\ p_i(k+1) = p_i(k) + v_i(k+1) \end{cases} \tag{62}$$

where $v_i(k)$ is the velocity of the ith particle at iteration k; w is a weighting function; c_1 and c_2 are acceleration factors; rand is a random number distributed in the interval [0, 1]; $\mathrm{pbest}\ _i$ and $\mathrm{gbest}\ _i$ are the best positions of personal particles and the best positions of all particles of the population, respectively; and $p_i(k)$ is the current position of the ith particle at the kth iteration.

5.2. Gravitational Search Algorithm

GSA is a population optimization algorithm based on the law of gravity and Newton's second law developed by Rashedi et al. [45]. It treats the solution to the optimization problem as a set of particles running in space [46]. The particles are attracted to each other through the action of gravity, which causes the particles to move toward the particle with the largest mass. The particle with the largest mass occupies the optimal position to find

the optimal solution to the optimization problem. The algorithm achieves the sharing of optimization information through the gravitational interaction between individuals and guides the group to search toward the optimal solution region [47].

In a D-dimensional search space, suppose there are N particles, and define the position of the ith particle as shown as Equation (63):

$$P_i = \left(p_i^1, \ldots, p_i^d, \ldots, p_i^d\right), i = 1, 2, \ldots, N \tag{63}$$

where p_i^d represents the position of the ith particle in dimension d.

In the GSA algorithm, the particle updates its velocity and position according to the Equation (64) for each process iteration:

$$\begin{cases} v_i^d(k+1) = \text{rand}_i \cdot v_i^d(k) + a_i^d(k) \\ p_i^d(k+1) = p_i^d(k) + v_i^d(k+1) \end{cases} \tag{64}$$

$$a_i^d(k) = \frac{F_i^d(k)}{M_i(k)} \tag{65}$$

where $p_i^d(k)$, $v_i^d(k)$, and $a_i^d(k)$ are the position, velocity, and acceleration of particle i in d dimension at the kth iteration, respectively; rand_i is a random number distributed in the interval [0, 1]; $F_i^d(k)$ is the magnitude of the force on particle i in d dimension at the kth iteration, which comes from the sum of all other particle forces; and $M_i(k)$ is the inertial mass of particle i at the kth iteration.

$$F_i^d(k) = \sum_{j=1, j \neq i}^{N} \text{rand}_j F_{ij}^d(k) \tag{66}$$

$$F_{ij}^d(k) = G(k) \frac{M_i(k) \cdot M_j(k)}{R_{ij}(k) + \varepsilon} \left(p_j^d(k) - p_i^d(k)\right) \tag{67}$$

where $F_{ij}^d(k)$ is the gravitational force of particle j on particle i at the kth iteration, rand_j is a random number distributed in the interval [0, 1], $G(k)$ is the gravitational constant at the kth iteration, $R_{ij}(k)$ is the Euclidean distance between particle j and particle i at the kth iteration, and ε is a small constant.

The inertial mass $M_i(k)$ of particle i at the kth iteration can be obtained from the following equation:

$$m_i(k) = \frac{fit_i(k) - \text{worst}(k)}{\text{best}(k) - \text{worst}(k)} \tag{68}$$

$$M_i(k) = \frac{m_i(k)}{\sum_{j=1}^{N} M_i(k)} \tag{69}$$

where $fit_i(k)$ is the size of the adaptation value of the ith particle at the kth iteration. For the HTGS problem, $\text{best}(k)$ and $\text{worst}(k)$ can be defined as follows:

$$\begin{cases} \text{best}(k) = \min fit_i(k), \ i \in \{1, 2, \ldots, N\} \\ \text{worst}(k) = \max fit_i(k), \ i \in \{1, 2, \ldots, N\} \end{cases} \tag{70}$$

The GSA algorithm has a strong global search capability but its local search capability is insufficient and it is prone to the oscillation of the optimal value.

5.3. Modified Hybrid Particle Swarm Optimization and Gravitational Search Algorithm with Chaotic Maps (CPSOGSA)

The hybrid PSOGSA was first developed by Mirjalili and Hashim [48], combining the advantages of PSO and GSA algorithms, and it is shown as Equation (71):

$$\begin{cases} v_i(k+1) = w \cdot v_i(k) + c_1^{'} \cdot \text{rand} \cdot a_i(k) + c_2^{'} \cdot \text{rand} \cdot (\text{gbest} - p_i(k)) \\ p_i(k+1) = p_i(k) + v_i(k+1) \end{cases} \tag{71}$$

When using chaotic maps in optimization algorithms, it is possible to quickly converge on the optimal solution and escape from the local optimal solution [49,50]. Therefore, the use of the chaotic mapping method in hybrid PSOGSA gives this algorithm the above advantages to improve the performance of PSOGSA.

The total force is calculated in Equation (66), using a random number from 0 to 1 as the weight, which means this random number affects the local search ability of the algorithm. Using the chaotic mapping method instead of random numbers can improve the convergence ability of the hybrid PSOGSA algorithm in the optimization process. Applying the chaotic mapping method to the total force values is shown in Equation (72). We use Equation (72) instead of random numbers to calculate the total force. After calculating the total force, the acceleration is determined using Equation (65), while the velocities and positions of all particles in the population are updated using Equation (71). The chaotic mapping methods used are from the ten chaotic maps shown in Table 1 and no random values exist in all chaotic maps [51].

$$F_i^d(k) = \sum_{j \in k\ best, j \neq i} C(k) F_{ij}^d(k) \tag{72}$$

Table 1. The chaotic mapping method.

No	Chaotic Map	Function	Range
1	Chebyshev	$y_{k+1} = \cos\left(k \cos^{-1}(y_k)\right)$	$[-1, 1]$
2	Circle	$y_{k+1} = mod\left(\left(y_k + d - \left(\frac{e}{2\pi}\right)\sin(2\pi y_k)\right), 1\right)$	$[0, 1]$
3	Gauss/Mouse	$y_{k+1} = \begin{cases} 1 & y_k = 0 \\ \frac{1}{mod(y_k, 1)} & \text{otherwise} \end{cases}$	$[0, 1]$
4	Iterative	$y_{k+1} = \sin\left(\frac{e\pi}{y_k}\right) e = 0.7$	$[-1, 1]$
5	Logistic	$y_{k+1} = e y_k (1 - y_k) e = 4$	$[0, 1]$
6	Piecewise	$y_{k+1} = \begin{cases} \frac{y_k}{M} & 0 \le y_k < M \\ \frac{y_k - M}{0.5 - M} & M \le y_k < 0.5 \\ \frac{1 - M - y_k}{0.5 - M} & 0.5 \le y_k < 1 - M \\ \frac{1 - y_k}{M} & 1 - M \le y_k < 1 \end{cases} M = 0.4$	$[0, 1]$
7	Sine	$y_{k+1} = \frac{e}{4}\sin(\pi y_k) e = 4$	$[0, 1]$
8	Singer	$y_{k+1} = \tau\left(7.86 y_k - 23.31 y_k^2 + 28.75 y_k^3 - 13.302875 y_k^4\right)$ $\tau = 1.07$	$[0, 1]$
9	Sinusoidal	$y_{k+1} = e y_k^2 \sin(\pi y_k) \quad e = 2.3$	$[0, 1]$
10	Tent	$y_{k+1} = \begin{cases} \frac{y_k}{0.7} & y_k < 0.7 \\ \frac{10}{3}(1 - y_k) & y_k \ge 0.7 \end{cases}$	$[0, 1]$

5.4. Optimal Feedback Coefficients for State Feedback Controller

For the mixed H_2/H_∞ controller $u(t) = \boldsymbol{K}_i \boldsymbol{x}(t)$, $(i = 1 \sim 3)$ designed in Section 4, the procedure for finding the optimal feedback coefficient $\boldsymbol{K}_i$ using CPSOGSA is given in this section.

The HTGS state space models corresponding to Equations (27), (32) and (37) were established in Simulink and the error performance indicators (adaptation values) were established at the same time, as shown in Figure 4. The commonly used error performance

indicators include ISE, IAE, ITAE, ISTE, etc. [52,53]. In this work, the ITAE indicator was selected, which is defined as follows:

$$fit = \int_0^\infty t|e(t)|dt \tag{73}$$

where $e(t)$ is the error.

The complete process is shown in Figures 5 and 6: CPSOGSA is assigned to the weighting coefficients $\mu_1^{(i)} \sim \mu_{10}^{(i)} \rightarrow$ the LMI toolbox in MATLAB is used to solve the mixed H_2/H_∞ controller feedback coefficients $\boldsymbol{K}_i \rightarrow \boldsymbol{K}_i$ is updated to the HTGS state-space model in Simulink for the characteristic test and the output adaptation value fit is calculated $\rightarrow$ the next round of $\mu_1^{(i)} \sim \mu_{10}^{(i)}$ assignment is carried out in the direction of minimizing fit, i.e., iterative optimization until the set number of iterations is reached.

The obtained set of $\mu_1^{(i)} \sim \mu_{10}^{(i)}$ with the smallest fit and the corresponding $\boldsymbol{K}_i$ are the optimal weighting and feedback coefficients, respectively. With this process, the optimal feedback coefficients $\boldsymbol{K}_1$, $\boldsymbol{K}_2$, and $\boldsymbol{K}_3$ are calculated. Finally, the HTGS T-S fuzzy mixed H_2/H_∞ controller based on the CPSOGSA optimization algorithm is obtained by substituting $\boldsymbol{K}_1$, $\boldsymbol{K}_2$, and $\boldsymbol{K}_3$ into Equation (44).

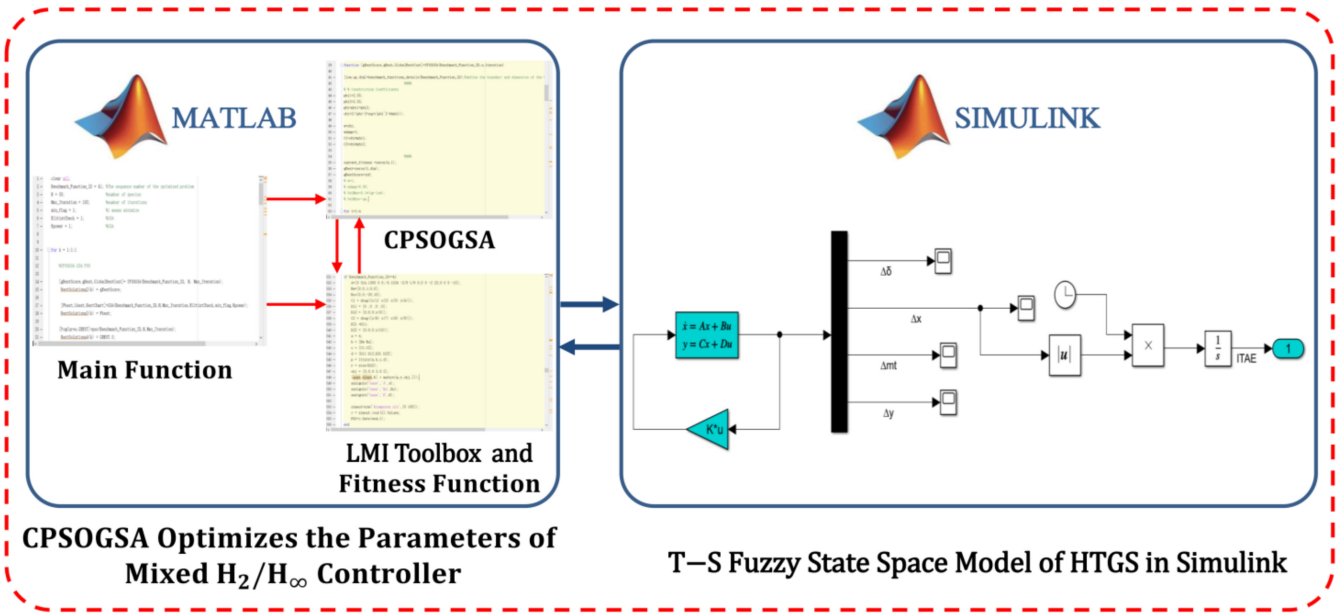

Figure 5. Schematic view of MATLAB/Simulink-based HTGS problem.

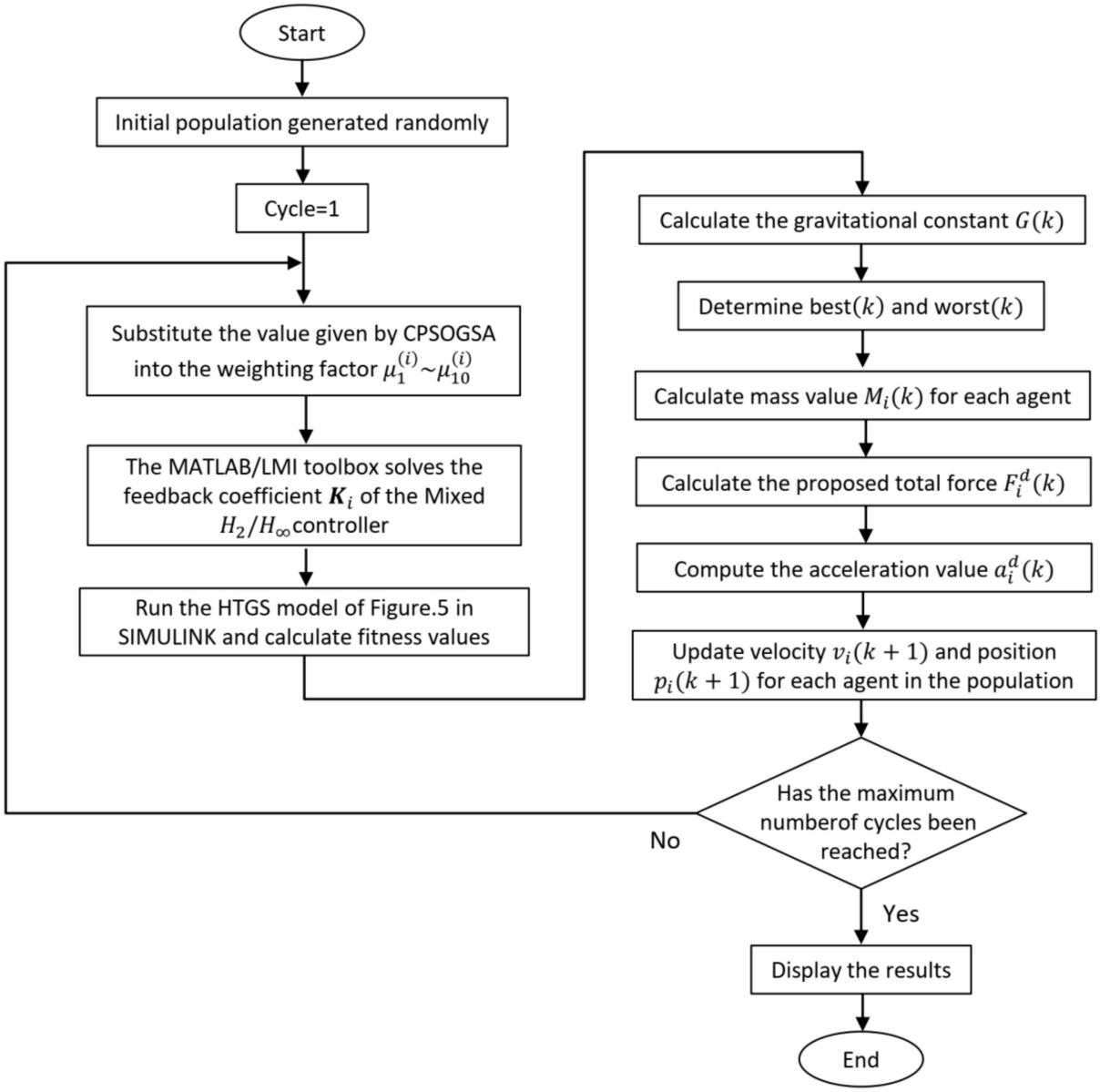

Figure 6. Solution process of CPSOGSA algorithm.

6. Simulation Studies

6.1. Model

According to Equations (2), (4), (11), (14), (20) and (44), the simulation models were built in Simulink. Figure 7 shows the simulation model of the hydraulic turbine, Figure 8 shows the simulation model of the penstock, Figure 9 shows the nonlinear simulation model of the generator, Figure 10 shows the simulation model of the actuator, Figure 11 shows the simulation model of the controller, and Figure 12 shows the simulation model of the HTGS.

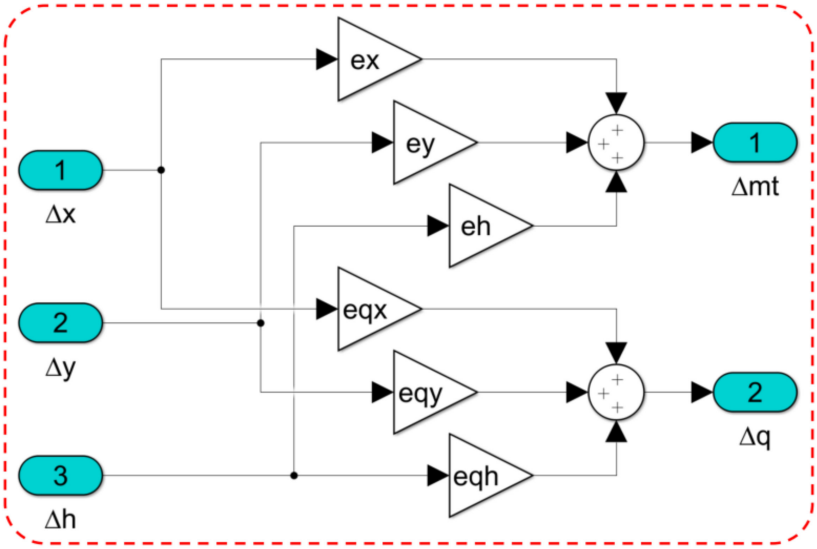

Figure 7. Simulation model of hydraulic turbine.

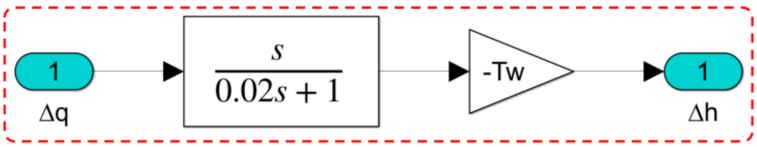

Figure 8. Simulation model of penstock.

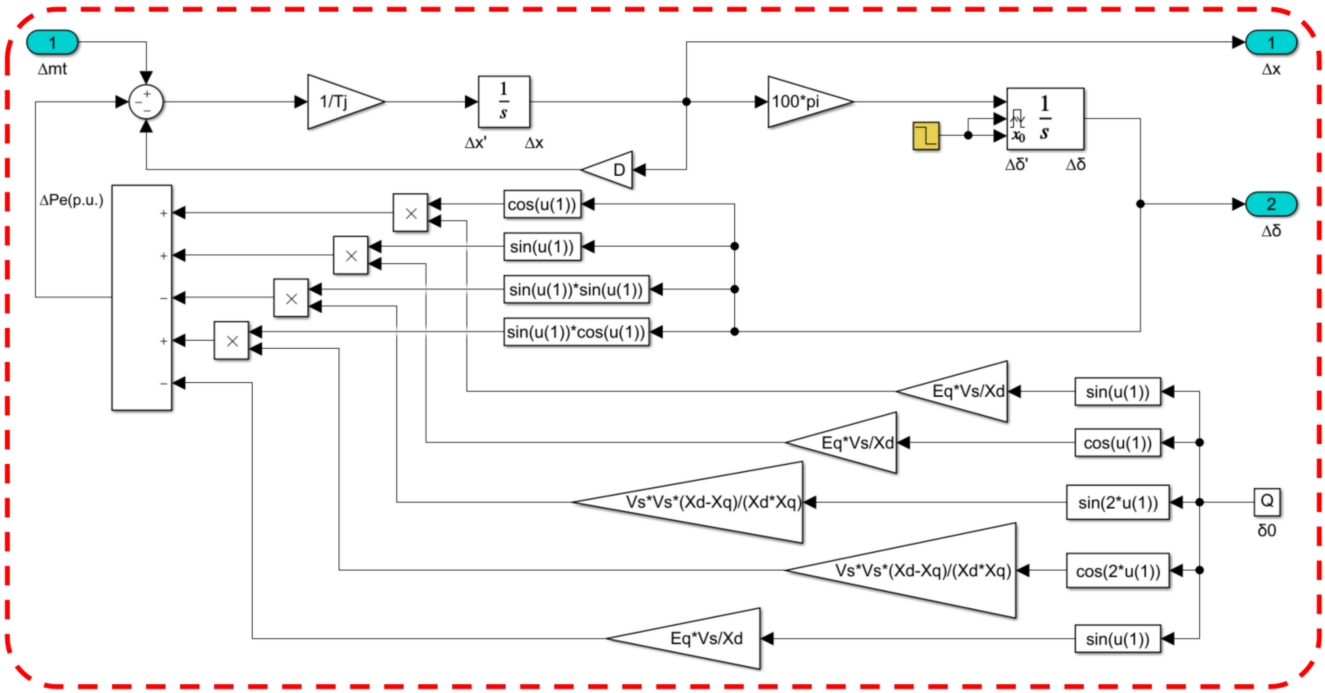

Figure 9. Simulation model of generator.

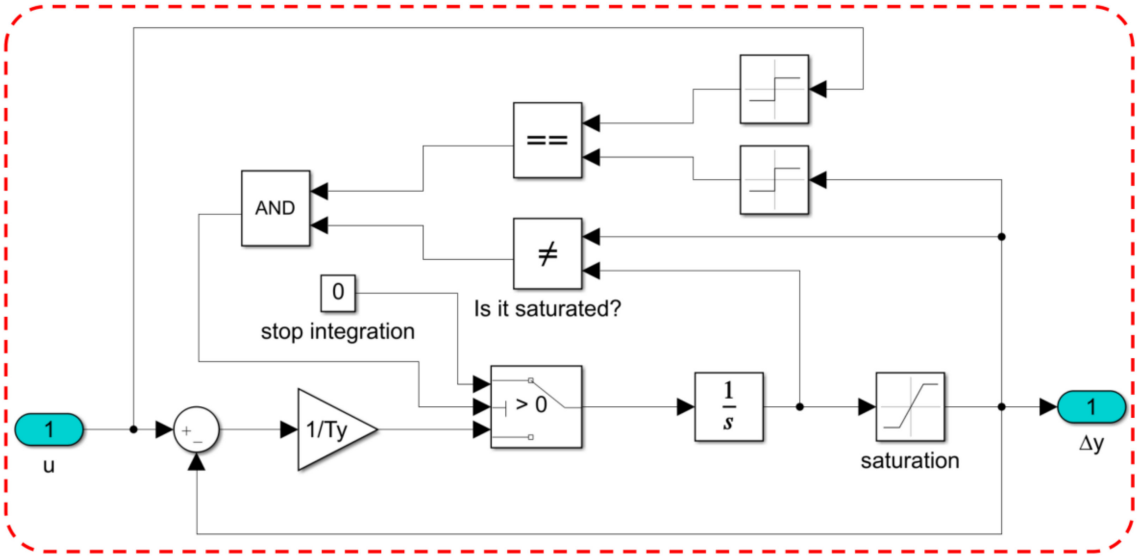

Figure 10. Simulation model of actuator.

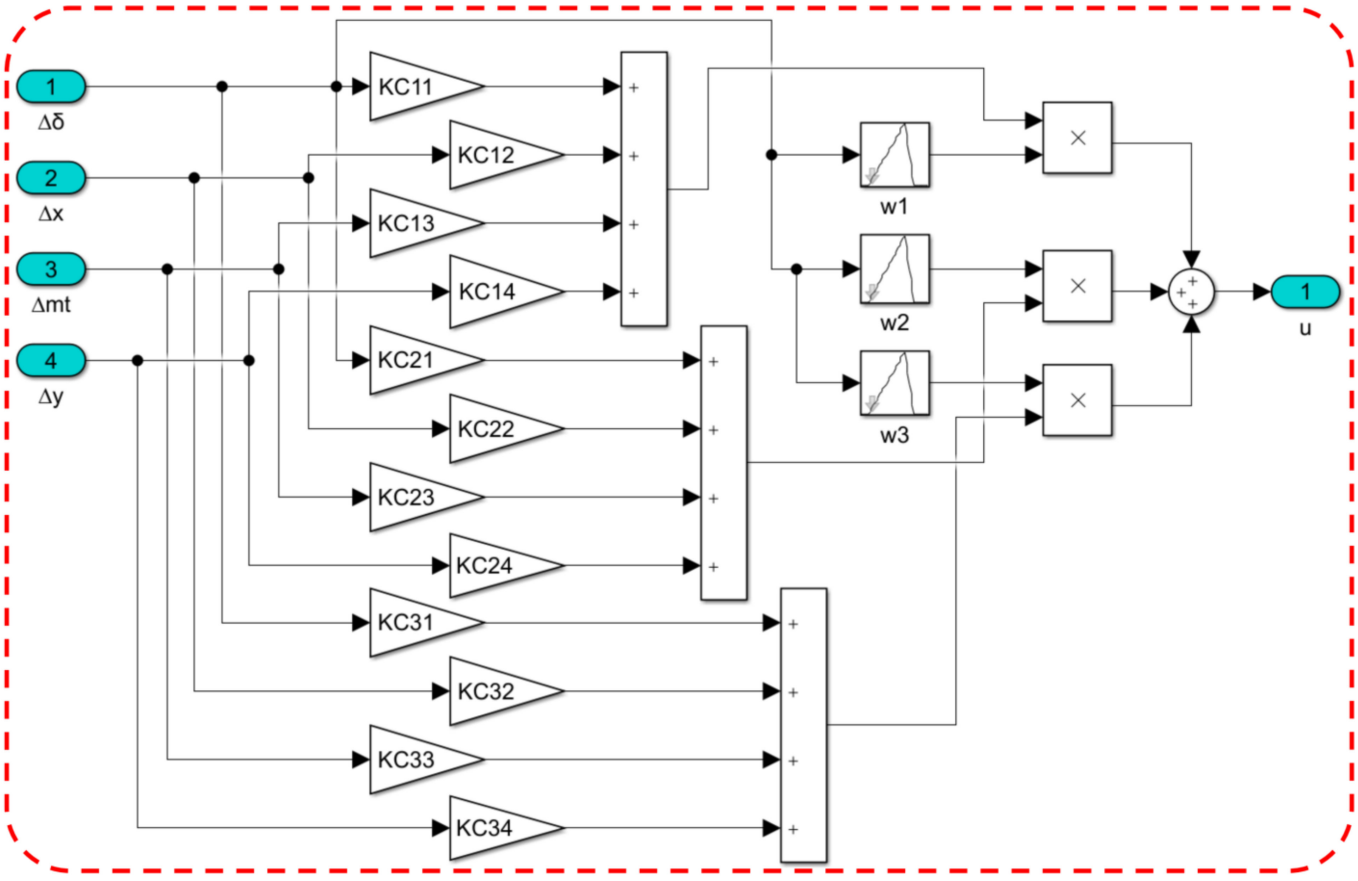

Figure 11. Simulation model of controller.

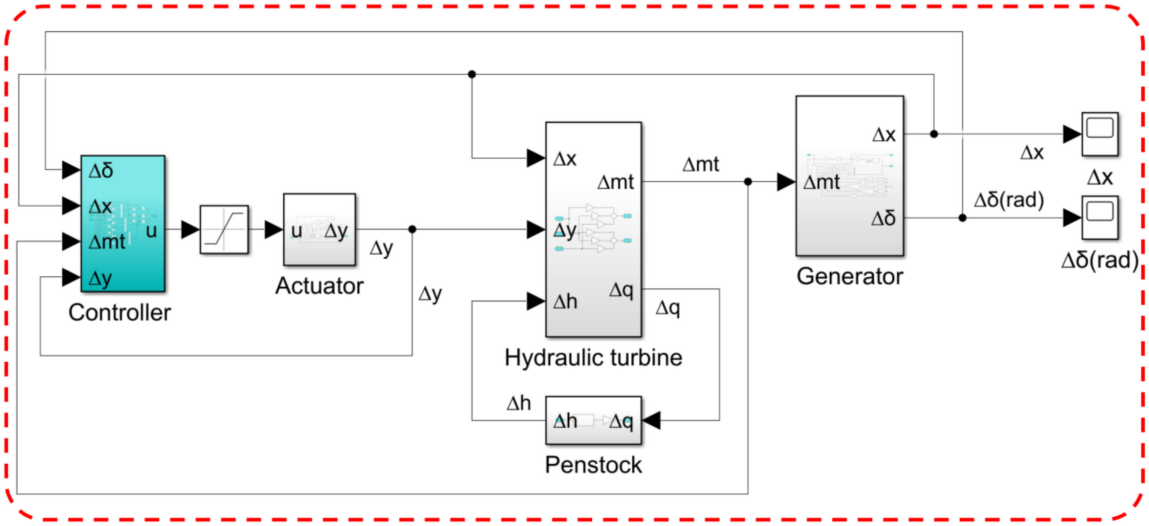

Figure 12. Simulation model of HTGS.

6.2. Parameters

The simulation test process is done in a MATLAB/Simulink environment. The main parameters of the HTGS in this paper are shown in Table 2.

Table 2. Parameters of HTGS.

Parameters	Value	Parameters	Value
e_x	−1.0	D	2.0
e_y	1.0	$E_q^{'}$	1.35
e_h	1.5	V_s	1.0
e_{qx}	0	$X_{D\Sigma}^{'}$	1.15
e_{qy}	1.0	$X_{q\Sigma}$	1.47
e_{qh}	0.5	$\delta_0(^\circ)$	30
e	1.0	T_w(s)	1.0
T_J(s)	9.0	T_y(s)	0.1

The corresponding matrix is as follows:

$$A^{(1)} = \begin{bmatrix} 0 & 314.1593 & 0 & 0 \\ -14.159 & -\frac{2}{9} & \frac{1}{9} & 0 \\ 0 & 0 & -1 & 22 \\ 0 & 0 & 0 & -24 \end{bmatrix} \tag{74}$$

$$A^{(2)} = \begin{bmatrix} 0 & 314.1593 & 0 & 0 \\ -14.159 & -\frac{2}{9} & \frac{1}{9} & 0 \\ 0 & 0 & -1 & 22 \\ 0 & 0 & 0 & -24 \end{bmatrix} \tag{75}$$

$$A^{(3)} = \begin{bmatrix} 0 & 314.1593 & 0 & 0 \\ -14.159 & -\frac{2}{9} & \frac{1}{9} & 0 \\ 0 & 0 & -1 & 22 \\ 0 & 0 & 0 & -24 \end{bmatrix} \tag{76}$$

$$B_u^{(1)} = B_u^{(2)} = B_u^{(3)} = \begin{bmatrix} 0 \\ 0 \\ -20 \\ 10 \end{bmatrix} \tag{77}$$

We set the number of optimization iterations to 100. The iterative process is shown in Figure 13. The CPSOGSA algorithm is close to convergence at the 80th iteration and the traditional PSO, GSA, and DE algorithms all fall into the local optimum problem. The adaptation value obtained by the CPSOGSA algorithm is the smallest compared to other optimization algorithms, which indicates that the CPSOGSA algorithm has more accurate computational results in the problem of optimizing the parameters of the HTGS mixed H_2/H_∞ controller.

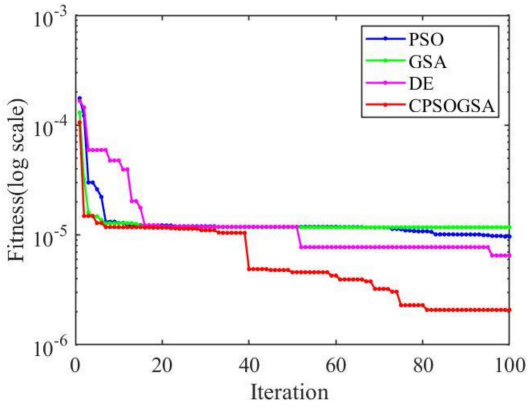

Figure 13. Convergence curve of controller optimization.

The weighting coefficients in Equations (49)–(54) obtained from the CPSOGSA optimization algorithm are shown in Table 3.

Table 3. Weighting coefficients.

Parameters	Value	Parameters	Value	Parameters	Value
$\mu_1^{(1)}$	0.0001	$\mu_1^{(2)}$	0.5441	$\mu_1^{(3)}$	0.8000
$\mu_2^{(1)}$	0.6607	$\mu_2^{(2)}$	0.6039	$\mu_2^{(3)}$	0.3319
$\mu_3^{(1)}$	0.7500	$\mu_3^{(2)}$	0.0134	$\mu_3^{(3)}$	0.0490
$\mu_4^{(1)}$	0.1500	$\mu_4^{(2)}$	0.4867	$\mu_4^{(3)}$	0.0915
$\mu_5^{(1)}$	0.0002	$\mu_5^{(2)}$	0.0288	$\mu_5^{(3)}$	0.0165
$\mu_6^{(1)}$	1.0000	$\mu_6^{(2)}$	0.4352	$\mu_6^{(3)}$	0.4000
$\mu_7^{(1)}$	0.0001	$\mu_7^{(2)}$	0.5438	$\mu_7^{(3)}$	0.9824
$\mu_8^{(1)}$	0.0010	$\mu_8^{(2)}$	0.0001	$\mu_8^{(3)}$	0.0001
$\mu_9^{(1)}$	0.1500	$\mu_9^{(2)}$	0.0008	$\mu_9^{(3)}$	0.0020
$\mu_{10}^{(1)}$	0.0001	$\mu_{10}^{(2)}$	0.0001	$\mu_{10}^{(3)}$	0.0001

The LMI toolbox in MATLAB is used to solve for the mixed H_2/H_∞ controller feedback coefficients with the following results:

$$\begin{cases} K_1 = \begin{bmatrix} 9,744 & 20,102 & -6,631 & -14,763 \end{bmatrix} \\ K_2 = \begin{bmatrix} 4,130 & -127,380 & -6,700 & -13,460 \end{bmatrix} \\ K_3 = \begin{bmatrix} 3,520 & -140,440 & -6,210 & -12,470 \end{bmatrix} \end{cases} \tag{78}$$

The HTGS T-S fuzzy mixed H_2/H_∞ controller based on CPSOGSA optimization is obtained by substituting $\boldsymbol{K}_1 \sim \boldsymbol{K}_3$ into Equation (44).

To demonstrate the performance feasibility of the controller in this paper, a T-S fuzzy linear quadratic regulator (LQR) controller and a PID controller are introduced for comparative analysis. The T-S fuzzy LQR controller was calculated according to the Q and

R matrices of the corresponding δ in the literature [54]. The Q and R matrices and the controller feedback coefficients K_{LQRi} are as follows:

$$Q_1 = Q_3 = \begin{bmatrix} 100 & 0 & 0 & 0 \\ 0 & 100 & 0 & 0 \\ 0 & 0 & 1 & 0 \\ 0 & 0 & 0 & 1 \end{bmatrix} \tag{79}$$

$$R_1 = R_3 = 0.1 \tag{80}$$

$$Q_2 = \begin{bmatrix} 48.261 & 0 & 0 & 0 \\ 0 & 230.5023 & 0 & 0 \\ 0 & 0 & 1.0182 & 0 \\ 0 & 0 & 0 & 9.9641 \end{bmatrix} \tag{81}$$

$$R_2 = 0.0337 \tag{82}$$

$$\begin{cases} K_{LQR1} = \begin{bmatrix} 30.7228 & 294.4374 & -19.5328 & -47.4211 \end{bmatrix} \\ K_{LQR2} = \begin{bmatrix} 35.6551 & 621.2588 & -23.7333 & -68.2293 \end{bmatrix} \\ K_{LQR3} = \begin{bmatrix} 30.6314 & 319.9401 & -18.4982 & -45.3461 \end{bmatrix} \end{cases} \tag{83}$$

6.3. Simulation and Validation Results

6.3.1. Case 1. Sudden Load Reduction

The variation curves of the rotational speed and unbalanced power of the unit for a sudden 0.2 (p.u.) load reduction of the system at 0.5 s are given in Figures 14 and 15, respectively. The solid red line is the simulation waveform of the controller obtained by the method shown in this paper. The green and blue dashed lines are the simulation waveforms with the T-S fuzzy LQR controller and without any controller, respectively. As shown in Figure 14, after the sudden load shedding, the rotational speed of unit rises to the maximum value within 0.5 s. If no controller is set, the rotational speed oscillates and decays with high fluctuation amplitude only under the effect of generator damping winding. With the T-S fuzzy LQR controller and the T-S fuzzy mixed H_2/H_∞ controller, the increase of the unit's rotational speed is slight and all of them can recover to the rated value. Compared to the T-S fuzzy LQR controller, the T-S fuzzy mixed H_2/H_∞ controller can stabilize the unit's rotational speed in a shorter interval with a transient time of Ts = 1.5 s. The performance indicators are compared as shown in Table 4. As shown in Figure 15, the T-S fuzzy mixed H_2/H_∞ controller can eliminate the unbalanced power quickly and has a smaller overshoot.

Table 4. Comparison of performance indicators of different controllers in Case 1.

	T-S Fuzzy LQR Controller	**T-S Fuzzy Mixed H_2/H_∞ Controller**
Overshoot (p.u.)	1.00155	1.00153
Transient time (s)	3.5	1.5

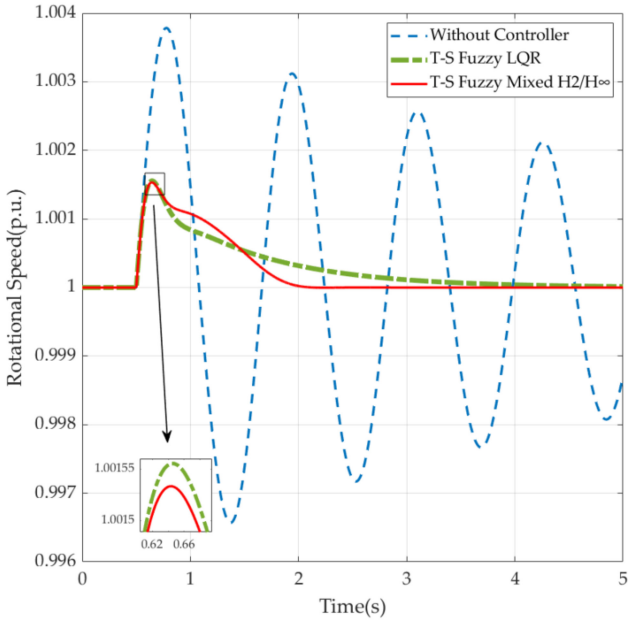

Figure 14. The curve of unit's rotational speed change during sudden 0.2 (p.u.) load reduction.

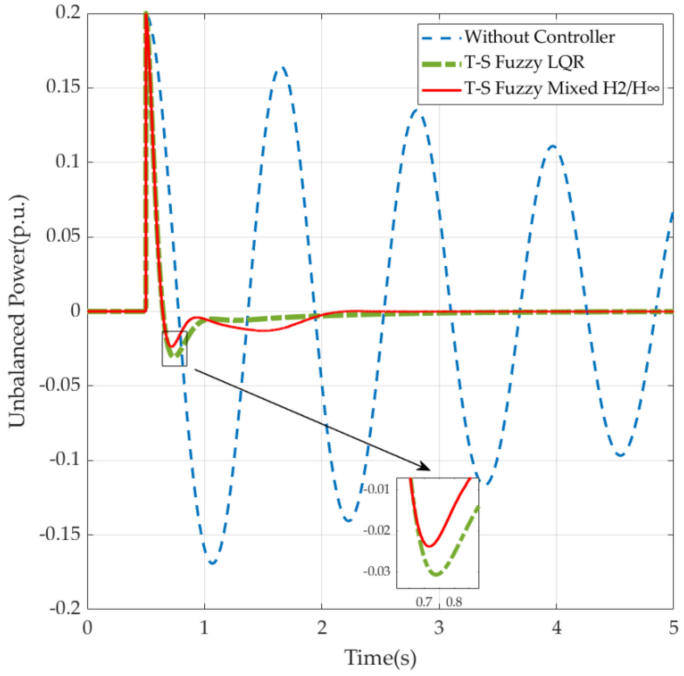

Figure 15. The curve of unbalanced power change during sudden 0.2 (p.u.) load reduction.

6.3.2. Case 2. Sudden Load Increase

The variation curves of the rotational speed and unbalanced power of the unit for a sudden 0.2 (p.u.) load increase of the system at 0.5 s are given in Figures 16 and 17, respectively. As shown in Figure 16, the rotational speed of the unit drops to the minimum value within 0.5 s after the sudden load increase. Without the controller, the rotational speed undergoes oscillatory decay with high fluctuation amplitude only under the effect of the generator damping winding. With the T-S fuzzy LQR controller and the T-S fuzzy mixed H_2/H_∞ controller, the reduction of the unit's rotational speed is slight and all of them can recover to the rated value. Compared to the T-S fuzzy LQR controller, the T-S fuzzy mixed H_2/H_∞ controller can stabilize the unit's rotational speed in a shorter interval

with a transient time of Ts = 1.3 s. The performance indicators are compared as shown in Table 5. As shown in Figure 17, the T-S fuzzy mixed H_2/H_∞ controller can eliminate the unbalanced power quickly and has a smaller overshoot.

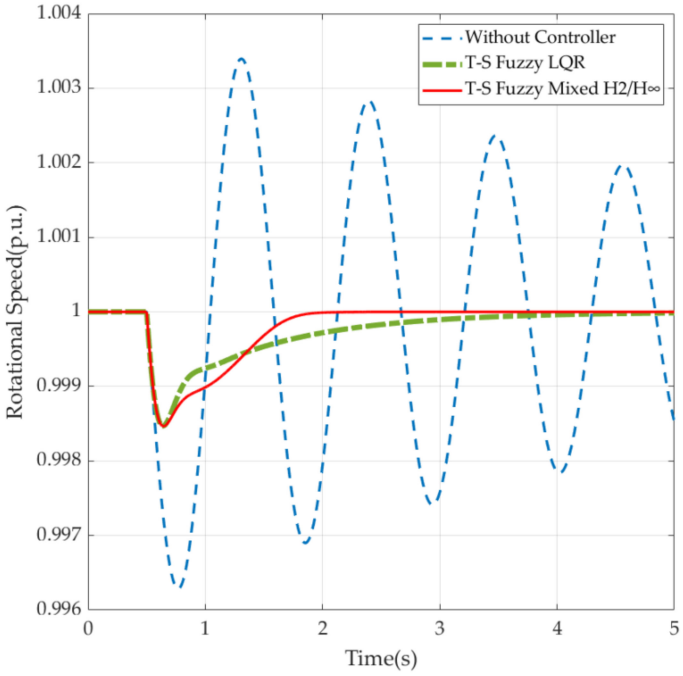

Figure 16. The curve of unit's rotational speed change during sudden 0.2 (p.u.) load increase.

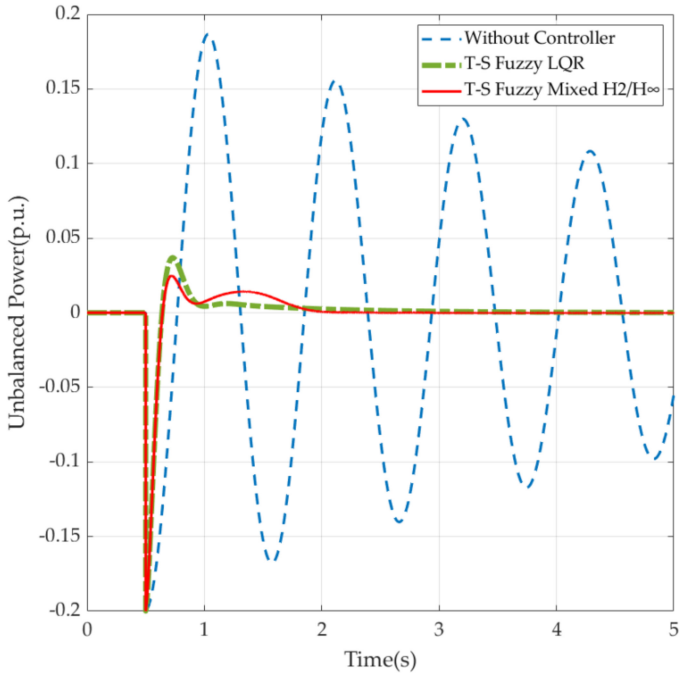

Figure 17. The curve of unbalanced power change during sudden 0.2 (p.u.) load increase.

Table 5. Comparison of performance indicators of different controllers in Case 2.

	T-S Fuzzy LQR Controller	**T-S Fuzzy Mixed H_2/H_∞ Controller**
Overshoot (p.u.)	0.9985	0.9985
Transient time (s)	4.5	1.3

6.3.3. Case 3. Perturbation from Wind Power

Simulations of the above two single load power disturbance cases show that the controller proposed in this paper has better control performance. Case 3 introduces the continuous wind power fluctuations depicted in Figure 18 to compare the proposed controller with the conventional PID controller. From the system frequency response shown in Figure 19, the proposed controller has better performance in suppressing the system frequency deviation caused by wind power fluctuation.

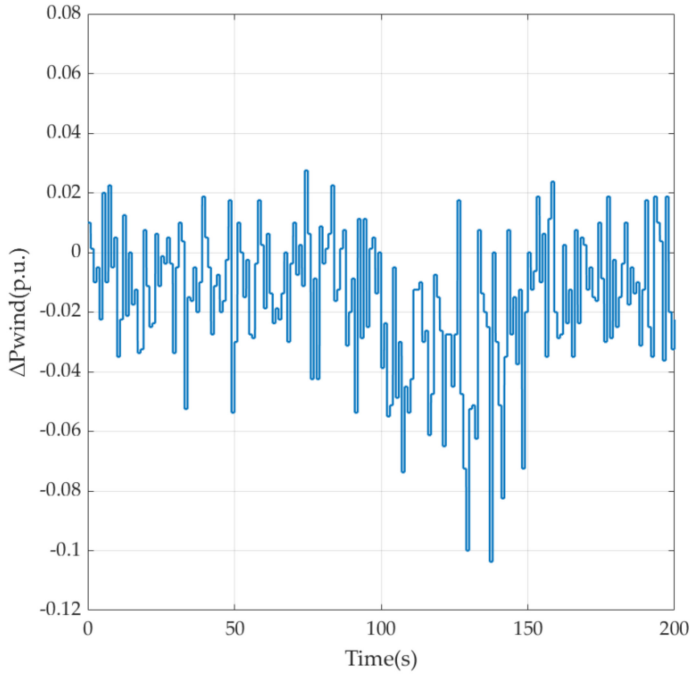

Figure 18. Continuous wind power fluctuations.

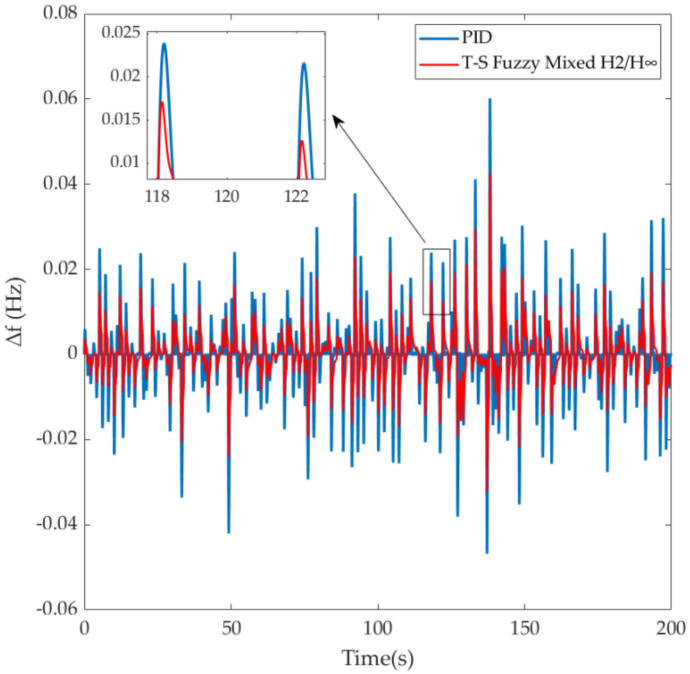

Figure 19. Frequency response of the system.

6.3.4. Case 4. System Parameters Change

As the hydro-generator set runs for a long time, some parameters change, which can affect the control performance of the controller. To illustrate the robustness of the designed controller, sensitivity analysis was performed by varying the system parameters in a simulation scenario. The variation of the control effect of the T-S fuzzy mixed H_2/H_∞ controller on the unit for a given δ disturbance when the actuator response time constant T_y and the penstock flowing water inertia time constant T_w are increased, shown in Figures 20 and 21 and Figures 22 and 23, respectively. As shown in Figures 20 and 21, the control effect of the proposed controller is almost unaffected when T_y increases. As shown in Figures 22 and 23, the rise of T_w has only a tiny impact on the overshoot amount, and the change of transient time is not apparent, all within the controllable range. It shows that the controller proposed in this paper can provide favorable control of the system with strong robustness, even in the case of unit parameter ingestion.

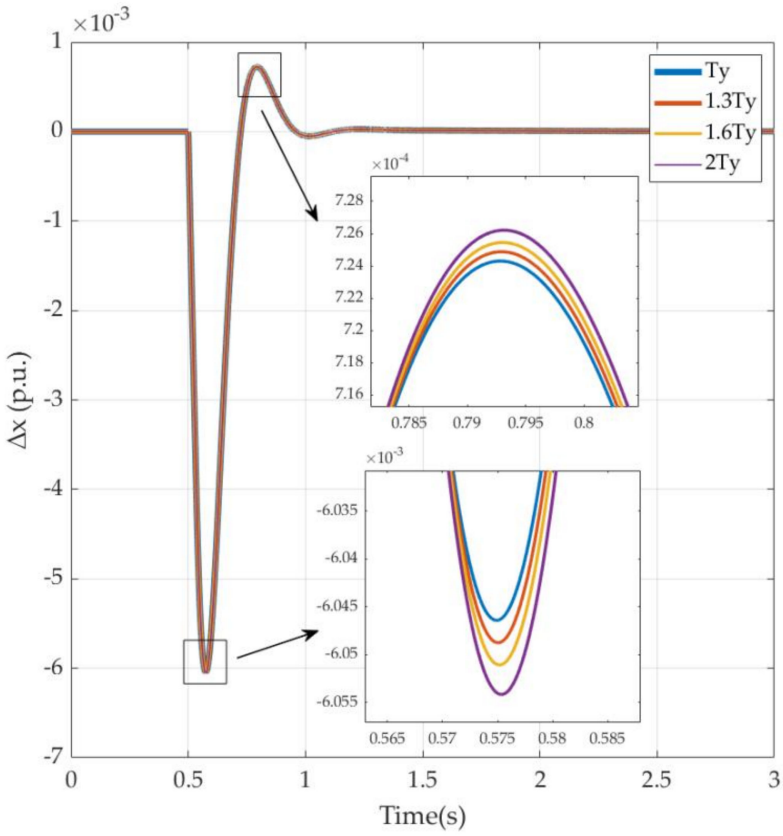

Figure 20. The control effect of the controller when T_y changes $(\Delta x - t)$.

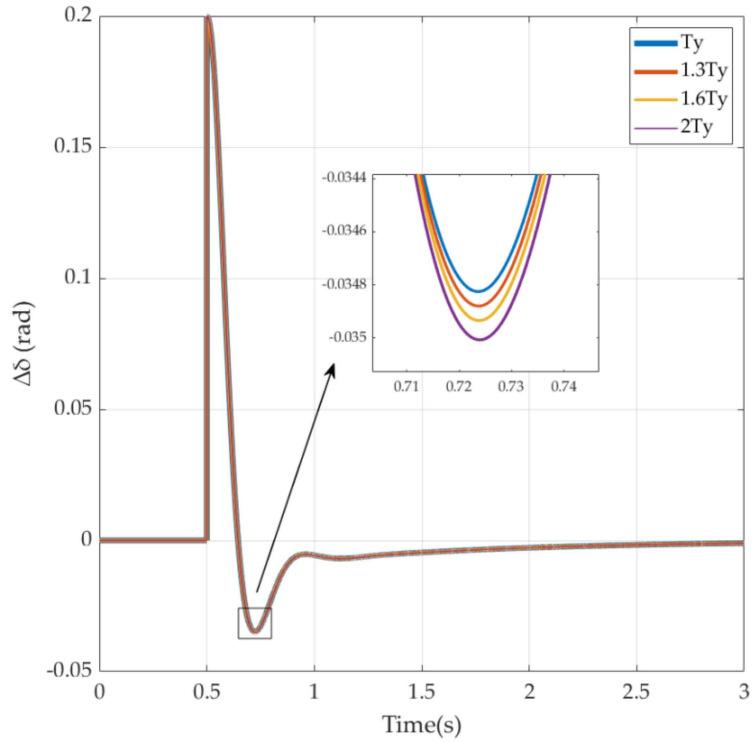

Figure 21. The control effect of the controller when T_y changes $(\Delta\delta - t)$.

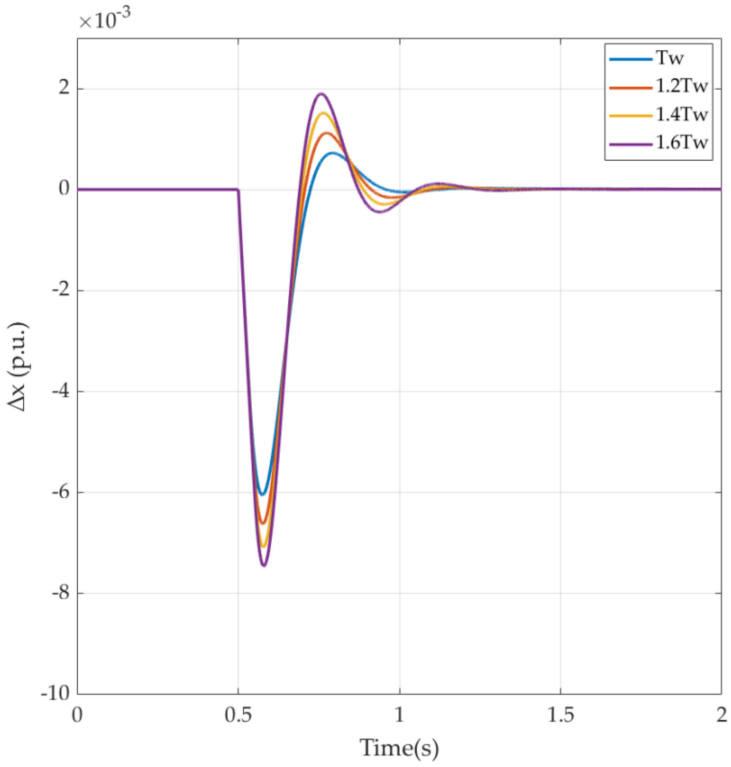

Figure 22. The control effect of the controller when T_w changes $(\Delta x - t)$.

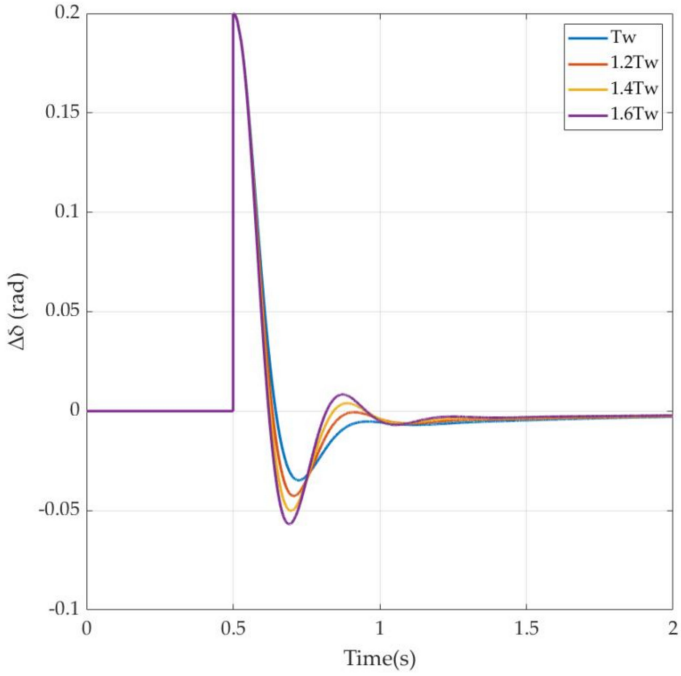

Figure 23. The control effect of the controller when T_w changes $(\Delta\delta - t)$.

7. Conclusions

To suppress the frequency fluctuations of the power system containing a hydro-generator set caused by load changes and the stochastic nature of renewable energy generation such as wind power, a T-S fuzzy mixed H_2/H_∞ controller for the hydraulic turbine governing system based on the CPSOGSA algorithm is proposed in this paper. Based on the study results, the following main conclusions can be drawn. (i) The CPSOGGSA algorithm is applicable to the optimization of the parameters associated with the proposed T-S fuzzy mixed H_2/H_∞ controller, which exhibits better performance in avoiding becoming trapped in a local optimum solution. (ii) This paper introduces an incremental form model of HTGS using precise electromagnetic power expressions to make the results of T-S fuzzy local linearization more accurate, which has not been proposed before. (iii) Simulation results show that the HTGS T-S fuzzy mixed H_2/H_∞ controller proposed in this paper outperforms existing state feedback controllers in terms of maximum overshoot and transient time in response to load variations and wind power perturbations. In addition, it is also verified that the method is highly robust to system parameter variations. It is our future work to study the load frequency control (LFC) of microgrids containing a hydro-generator set with the introduction of energy storage elements using the T-S fuzzy mixed H_2/H_∞ control method based on CPSOGSA.

Author Contributions: Conceptualization, L.L.; methodology, L.L. and J.Q.; software, L.L. and Y.Z. (Yidong Zou); validation, J.Q. and F.C.; formal analysis, D.T.; investigation, L.L.; resources, J.Q.; data curation, L.L. and Y.Z. (Yun Zeng); writing—original draft preparation, L.L. and Y.Z. (Yidong Zou); writing—review and editing, L.L. and J.Q.; visualization, X.L.; supervision, L.L.; project administration, L.L.; funding acquisition, J.Q. All authors have read and agreed to the published version of the manuscript.

Funding: This research was funded by the National Natural Science Foundation of China, grant number 51869007.

Institutional Review Board Statement: Not applicable.

Informed Consent Statement: Not applicable.

Data Availability Statement: Not applicable.

Conflicts of Interest: The authors declare no conflict of interest.

Abbreviations

HTGS	Hydraulic turbine governing system
T-S	Takagi–Sugeno
LMI	Linear matrix inequality
CPSOGSA	Modified hybrid particle swarm optimization and gravitational search algorithm with chaotic maps
LQR	Linear quadratic regulator
PID	Proportional-integral-derivative
PDC	Parallel distributed compensation
GSA	Gravitational search algorithm
PSO	Particle swarm optimization
GA	Genetic algorithm
LFC	Load frequency control

References

1. Zhang, D.; Wang, J.; Lin, Y.; Si, Y.; Huang, C.; Yang, J.; Huang, B.; Li, W. Present situation and future prospect of renewable energy in China. *Renew. Sustain. Energy Rev.* **2017**, *76*, 865–871. [CrossRef]
2. Li, X.-z.; Chen, Z.-j.; Fan, X.-c.; Cheng, Z.-j. Hydropower development situation and prospects in China. *Renew. Sustain. Energy Rev.* **2018**, *82*, 232–239. [CrossRef]
3. Guo, W.; Yang, J.; Wang, M.; Lai, X. Nonlinear modeling and stability analysis of hydro-turbine governing system with sloping ceiling tailrace tunnel under load disturbance. *Energy Convers. Manag.* **2015**, *106*, 127–138. [CrossRef]
4. Yang, J.; Wang, M.; Wang, C.; Guo, W. Linear Modeling and Regulation Quality Analysis for Hydro-Turbine Governing System with an Open Tailrace Channel. *Energies* **2015**, *8*, 11702–11717. [CrossRef]
5. Wang, C.; Wang, D.K.; Zhang, J.M. Experimental Study on the Optimal Strategy for of Governing System of Hydropower Station. *Water* **2021**, *13*, 421. [CrossRef]
6. Xu, B.; Jun, H.-B.; Chen, D.; Li, H.; Zhang, J.; Blanco, C.J.C.; Shen, H. Stability analysis of a hydro-turbine governing system considering inner energy losses. *Renew. Energy* **2019**, *134*, 258–266. [CrossRef]
7. Li, H.; Xu, B.; Arzaghi, E.; Abbassi, R.; Chen, D.; Aggidis, G.; Zhang, J.; Patelli, E. Transient safety assessment and risk mitigation of a hydroelectric generation system. *Energy* **2020**, *196*, 117135. [CrossRef]
8. Zeng, Y.; Qian, J.; Guo, Y.; Yu, S. Differential equation model of single penstock multi-machine system with hydraulic coupling. *IET Renew. Power Gener.* **2019**, *13*, 1153–1159. [CrossRef]
9. Zhang, H.; Chen, D.; Xu, B.; Wang, F. Nonlinear modeling and dynamic analysis of hydro-turbine governing system in the process of load rejection transient. *Energy Convers. Manag.* **2015**, *90*, 128–137. [CrossRef]
10. Wang, F.; Chen, D.; Xu, B.; Zhang, H. Nonlinear dynamics of a novel fractional-order Francis hydro-turbine governing system with time delay. *Chaos Solitons Fractals* **2016**, *91*, 329–338. [CrossRef]
11. Lai, X.; Li, C.; Zhou, J.; Zhang, Y.; Li, Y. A multi-objective optimization strategy for the optimal control scheme of pumped hydropower systems under successive load rejections. *Appl. Energy* **2020**, *261*, 114474. [CrossRef]
12. Fang, H.; Chen, L.; Shen, Z. Application of an improved PSO algorithm to optimal tuning of PID gains for water turbine governor. *Energy Convers. Manag.* **2011**, *52*, 1763–1770. [CrossRef]
13. Chen, Z.; Yuan, Y.; Yuan, X.; Huang, Y.; Li, X.; Li, W. Application of multi-objective controller to optimal tuning of PID gains for a hydraulic turbine regulating system using adaptive grid particle swam optimization. *ISA Trans.* **2015**, *56*, 173–187. [CrossRef]
14. Li, C.; Zhang, N.; Lai, X.; Zhou, J.; Xu, Y. Design of a fractional-order PID controller for a pumped storage unit using a gravitational search algorithm based on the Cauchy and Gaussian mutation. *Inf. Sci.* **2017**, *396*, 162–181. [CrossRef]
15. Junyi, L.; Chen, Q. Fractional Order Controller Designing with Firefly Algorithm and Parameter Optimization for Hydroturbine Governing System. *Math. Probl. Eng.* **2015**, *2015*, 1–11. [CrossRef]
16. Wang, B.; Xue, J.; Wu, F.; Zhu, D. Robust Takagi-Sugeno fuzzy control for fractional order hydro-turbine governing system. *Isa Trans.* **2016**, 72. [CrossRef]
17. Chen, Z.; Yuan, X.; Yuan, Y.; Lei, X.; Zhang, B. Parameter estimation of fuzzy sliding mode controller for hydraulic turbine regulating system based on HICA algorithm. *Renew. Energy* **2019**, *133*, 551–565. [CrossRef]
18. Chen, D.; Ding, C.; Do, Y.; Ma, X.; Zhao, H.; Wang, Y. Nonlinear dynamic analysis for a Francis hydro-turbine governing system and its control. *J. Frankl. Inst.* **2014**, *351*, 4596–4618. [CrossRef]
19. Zhang, Y.; Chen, T.; Li, J.; Yu, J. Experimental Study of Load Variations on Pressure Fluctuations in a Prototype Reversible Pump Turbine in Generating Mode. *J. Fluids Eng.* **2017**, *139*, 074501. [CrossRef]
20. Xu, B.; Chen, D.; Tolo, S.; Patelli, E.; Jiang, Y. Model validation and stochastic stability of a hydro-turbine governing system under hydraulic excitations. *Int. J. Electr. Power Energy Syst.* **2018**, *95*, 156–165. [CrossRef]

21. Li, H.; Chen, D.; Arzaghi, E.; Abbassi, R.; Kilicman, A.; Caraballo, T.; Patelli, E.; Gao, X.; Xu, B. Dynamic safety assessment of a nonlinear pumped-storage generating system in a transient process. *Commun. Nonlinear Sci. Numer. Simul.* **2019**, *67*, 192–202. [CrossRef]
22. Guo, B.; Xu, B.; Chen, D.; Ye, W.; Guo, P.; Luo, X. Dynamic modeling and energy distribution analysis in a hydroelectric generating system considering the stochastic turbine flow. *Int. J. Electr. Power Energy Syst.* **2018**, *103*, 611–621. [CrossRef]
23. Guo, W.; Yang, J. Modeling and dynamic response control for primary frequency regulation of hydro-turbine governing system with surge tank. *Renew. Energy* **2018**, *121*, 173–187. [CrossRef]
24. Rajendran, M.; Parthasarathy, P.; Anbumozhi, R. Robust Analysis of T-S Fuzzy Controller for Nonlinear System Using H-Infinity. In *Advanced Engineering Optimization Through Intelligent Techniques. Advances in Intelligent Systems and Computing*; Springer: Singapore, 2020; Volume 949, pp. 643–651. [CrossRef]
25. Hosseinzadeh, M.; Sadati, N.; Zamani, I. H∞ disturbance attenuation of fuzzy large-scale systems. In Proceedings of the 2011 IEEE International Conference on Fuzzy Systems (FUZZ-IEEE 2011), Taipei, Taiwan, 27–30 June 2011.
26. Taniguchi, T.; Tanaka, K.; Ohtake, H.; Wang, H.O. Model construction, rule reduction, and robust compensation for generalized form of Takagi-Sugeno fuzzy systems. *IEEE Trans. Fuzzy Syst.* **2002**, *9*, 525–538. [CrossRef]
27. Wang, B.; Xue, J.; Wu, F.; Zhu, D. Finite time takagi-sugeno fuzzy control for hydro-turbine governing system. *J. Vib. Control.* **2018**, *24*, 1001–1010. [CrossRef]
28. Gao, Q.; Zeng, X.J.; Feng, G.; Wang, Y.; Qiu, J. T-S-Fuzzy-Model-Based Approximation and Controller Design for General Nonlinear Systems. *IEEE Trans. Syst. Man Cybern. Part B Cybern.* **2012**, *42*, 1143–1154. [CrossRef]
29. Li, Y.; Yuan, H.; Yu, J.; Zhang, G.; Liu, K. A review of the application of genetic algorithms to optimization problems. *Shandong Ind. Technol.* **2019**, *12*, 242–243. [CrossRef]
30. Cheng, L.; Xue, Y. Optimization of Primary Frequency Modulation PID Parameters of Hydropower Unit Based on Particle Swarm Optimization. *Qinghai Electr. Power* **2019**, *38*, 27–30. [CrossRef]
31. Jiang, C.; Ma, Y.; Wang, C. PID controller parameters optimization of hydro-turbine governing systems using deterministic-chaotic-mutation evolutionary programming (DCMEP). *Energy Convers. Manag.* **2006**, *47*, 1222–1230. [CrossRef]
32. Yang, W.; Norrlund, P.; Saarinen, L.; Yang, J.; Lundin, U. Wear Reduction for Hydropower Turbines Considering Frequency Quality of Power Systems: A Study on Controller Filters. *IEEE Trans. Power Syst.* **2016**, *32*, 1191–1201. [CrossRef]
33. Guo, W.; Yang, J. Stability performance for primary frequency regulation of hydro-turbine governing system with surge tank. *Appl. Math. Model.* **2018**, *54*, 446–466. [CrossRef]
34. Wang, L.; Han, Q.; Chen, D.; Wu, C.; Wang, X. Non-linear modelling and stability analysis of the PTGS at pump mode. *Iet Renew. Power Gener.* **2017**, *11*, 827–836. [CrossRef]
35. Castronuovo, E.; Usaola, J.; Bessa, R.; Matos, M.; Costa, I.C.; Bremermann, L.; Lugaro, J.; Kariniotakis, G. An integrated approach for optimal coordination of wind power and hydro pumping storage. *Wind. Energy* **2014**, *17*, 829–852. [CrossRef]
36. Guo, B.; Guo, J. Feedback Linearization and Reaching Law Based Sliding Mode Control Design for Nonlinear Hydraulic Turbine Governing System. *Energies* **2019**, *12*, 2273. [CrossRef]
37. Yan, D.; Wang, W.; Chen, Q. Nonlinear Modeling and Dynamic Analyses of the Hydro–Turbine Governing System in the Load Shedding Transient Regime. *Energies* **2018**, *11*, 1244. [CrossRef]
38. Yang, Y.; Wang, B.; Tian, Y.; Chen, P. Fractional-Order Finite-Time, Fault-Tolerant Control of Nonlinear Hydraulic-Turbine-Governing Systems with an Actuator Fault. *Energies* **2020**, *13*, 3812. [CrossRef]
39. Tian, T.; Liu, C.; Guo, Q.; Yuan, Y.; Li, W.; Yan, Q. An Improved Ant Lion Optimization Algorithm and Its Application in Hydraulic Turbine Governing System Parameter Identification. *Energies* **2018**, *11*, 95. [CrossRef]
40. Takagi, T.; Sugeno, M. Fuzzy identification of systems and its applications to modeling and control. *IEEE Trans. Syst. Man Cybern.* **1985**, *SMC-15*, 116–132. [CrossRef]
41. Gahinet, P.; Nemirovskii, A.; Laub, A.J.; Chilali, M. The LMI control toolbox. In Proceedings of the IEEE Conference on Decision & Control, Las Vegas, NV, USA, 10–13 December 2002.
42. Gahinet, P.; Nemirovski, A.; Laub, A.J.; Chilali, M. *LMI Control Toolbox—For Use with MATLAB*; The MathWorks, Inc.: Natick, MA, USA, 1995.
43. Kennedy, J.; Eberhart, R. Particle Swarm Optimization. In Proceedings of the Icnn95-international Conference on Neural Networks, Perth, WA, Australia, 27 November–1 December 1995.
44. Cheng, X.; Chi, J. Optimization of Multi-core Task Scheduling based on Improved Particle Swarm Optimization Algorithm. In Proceedings of the ICIIP 2019 4th International Conference on Intelligent Information Processing, Guilin, China, 16–17 November 2019.
45. Rashedi, E.; Nezamabadi-pour, H.; Saryazdi, S. GSA: A Gravitational Search Algorithm. *Inf. Sci.* **2009**, *179*, 2232–2248. [CrossRef]
46. Zibanezhad, B.; Zamanifar, K.; Sadjady, R.S.; Rastegari, Y. Applying gravitational search algorithm in the QoS-based Web service selection problem. *J. Zhejiang Univ. Sci. C* **2011**, *12*, 730–742. [CrossRef]
47. Ma, L.; Zhang, P.; Ma, J. Mathematical Model for an Electrode-Type Electric Boiler Based on GSA-optimized Neural Network. In Proceedings of the 2018 14th International Conference on Natural Computation, Fuzzy Systems and Knowledge Discovery (ICNC-FSKD), Anhui, China, 28–30 July 2018.
48. Mirjalili, S.; Hashim, S. A new hybrid PSOGSA algorithm for function optimization. In Proceedings of the International Conference on Computer & Information Application, Taiyuan, China, 22–24 October 2010.

49. Gandomi, A.; Yang, X.-S.; Talatahari, S.; Alavi, A. Firefly algorithm with chaos. *Commun. Nonlinear Sci. Numer. Simul.* **2013**, *18*, 89–98. [CrossRef]
50. Gandomi, A.H.; Yang, X.-S. Chaotic bat algorithm. *J. Comput. Sci.* **2014**, *5*, 224–232. [CrossRef]
51. Duman, S.; Li, J.; Wu, L.; Guvenc, U. Optimal power flow with stochastic wind power and FACTS devices: A modified hybrid PSOGSA with chaotic maps approach. *Neural Comput. Appl.* **2020**, *32*, 8463–8492. [CrossRef]
52. Barisal, A.K. Comparative performance analysis of teaching learning based optimization for automatic load frequency control of multi-source power systems. *Int. J. Electr. Power Energy Syst.* **2015**, *66*, 67–77. [CrossRef]
53. Boulkaibet, I.; Belarbi, K.; Bououden, S.; Marwala, T.; Chadli, M. A new T-S fuzzy model predictive control for nonlinear processes. *Expert Syst. Appl.* **2017**, *88*, 132–151. [CrossRef]
54. Zou, Y.; Qian, J.; Zeng, Y.; Guo, Y.; Wu, M.; Wang, F.; Mei, H. Eigen-Structure Assignment-Based Differential Evolution Algorithm for T-S Fuzzy Control Tuning Applied to Water-Turbine Governing System. *IEEE Access* **2021**, *9*, 39322–39332. [CrossRef]